Circular RNA Vaccines against SARS-CoV-2 and Emerging Variants

Liang Qu[1]*, Zongyi Yi[1,2]*, Yong Shen[1,2]*, Liangru Lin[1], Feng Chen[2], Yiyuan Xu[1], Zeguang Wu[1], Huixian Tang[1], Xiaoxue Zhang[1,2], Feng Tian[1], Chunhui Wang[1], Xia Xiao[3], Xiaojing Dong[3], Li Guo[3], Shuaiyao Lu[4], Chengyun Yang[4], Cong Tang[4], Yun Yang[4], Wenhai Yu[4], Junbin Wang[4], Yanan Zhou[4], Qing Huang[4], Ayijiang Yisimayi[5], Yunlong Cao[5], Youchun Wang[6], Zhuo Zhou[1], Xiaozhong Peng[4,7], Jianwei Wang[3], Xiaoliang Sunney Xie[5], Wensheng Wei[1]†

[1]Biomedical Pioneering Innovation Center, Beijing Advanced Innovation Center for Genomics, Peking-Tsinghua Center for Life Sciences, Peking University Genome Editing Research Center, State Key Laboratory of Protein and Plant Gene Research, School of Life Sciences, Peking University, Beijing, P.R. China.

[2]Academy for Advanced Interdisciplinary Studies, Peking University, Beijing 100871, China.

[3]NHC Key Laboratory of Systems Biology of Pathogens and Christophe Mérieux Laboratory, Institute of Pathogen Biology, Chinese Academy of Medical Sciences and Peking Union Medical College, Beijing 100730, China; Key Laboratory of Respiratory Disease Pathogenomics, Chinese Academy of Medical Sciences and Peking Union Medical College, Beijing 100730, China.

[4]National Kunming High-level Biosafety Primate Research Center, Institute of Medical Biology, Chinese Academy of Medical Sciences and Peking Union Medical College, Yunnan China.

[5]Biomedical Pioneering Innovation Center, Beijing Advanced Innovation Center for Genomics, Peking-Tsinghua Center for Life Sciences, Peking University, Beijing 100871, China.

[6]Division of HIV/AIDS and Sex-transmitted Virus Vaccines, Institute for Biological Product Control, National Institutes for Food and Drug Control (NIFDC) and WHO Collaborating Center for Standardization and Evaluation of Biologicals, Beijing 102629, China.

[7]State Key Laboratory of Medical Molecular Biology, Department of Molecular Biology and Biochemistry, Institute of Basic Medical Sciences, Medical Primate Research Center, Neuroscience Center, Chinese Academy of Medical Sciences, School of Basic Medicine Peking Union Medical College, Beijing 100730, China.

*These authors contributed equally to this work.

†Correspondence: Wensheng Wei (wswei@pku.edu.cn).

Abstract: Severe acute respiratory syndrome coronavirus 2 (SARS-CoV-2) and its emerging variants of concern (VOC), such as Delta (B.1.617.2) and Omicron (B.1.1.529), has continued to drive the worldwide pandemic. Therefore, there is a high demand for vaccines with enhanced efficacy, high thermostability, superior design flexibility, and fast manufacturing speed. Here, we report a circular RNA (circRNA) vaccine that encodes the trimeric RBD of SARS-CoV-2 Spike protein. Without the need of nucleotide modification, 5'-capping or 3'-polyadenylation, circRNA could be rapidly produced via *in vitro* transcription and is highly thermostable whether stored in naked or lipid-nanoparticle (LNP)-encapsulated format. LNP-encapsulated circRNA^{RBD} elicited potent neutralizing antibodies and T cell responses, providing robust protection against Beta (B.1.351) and native viruses in mice and rhesus macaques, respectively. Notably, circRNA vaccine enabled higher and more durable antigen production than 1mΨ-modified mRNA vaccine, eliciting a higher proportion of neutralizing antibodies and stronger Th1-biased immune responses. Importantly, we found that circRNA$^{RBD\text{-}Omicron}$ vaccine induced effective neutralizing antibodies against only Omicron but not Delta variant. By contrast, circRNA$^{RBD\text{-}Delta}$ could elicit high level of neutralizing antibodies against both Delta and Omicron. Following two doses of either native- or Delta-specific vaccination, circRNA$^{RBD\text{-}Delta}$, but not Omicron or Beta vaccines, could effectively boost the neutralizing antibodies against both Delta and Omicron variants. These results suggest that circRNA$^{RBD\text{-}Delta}$ is a favorable choice for vaccination to provide a broad-spectrum protection against the current variants of concern of SARS-CoV-2.

Main Text:

Coronavirus disease 2019 (COVID-19) is a serious worldwide public health emergency caused by a novel severe acute respiratory syndrome coronavirus (SARS-CoV-2)[1,2]. So far, COVID-19 had resulted in ~300 million confirmed cases and over 5 million confirmed deaths (World Health Organization). With the development of the epidemic, variants with immune escape ability appeared, the most serious of which is Omicron. As of Dec. 28, 2021, Omicron had taken ~30% of COVID-19 cases (GISAID). The rapid rise of Omicron suggests that it could overtake Delta as

60 the next dominant strain. Omicron carries over 30 mutations on the Spike protein, 15 of which are
61 located in the receptor-binding domain (RBD)[3], resulting in a significant decrease in the
62 effectiveness of prior neutralizing antibodies[4-8]. This poses a severe challenge to the efficacy of
63 current vaccines, highlighting the urgent need to develop effective vaccines against such fast-
64 spreading variants.

65 SARS-CoV-2, together with the other two highly pathogenic coronaviruses, Severe Acute
66 Respiratory Syndrome (SARS)-CoV and Middle East Respiratory Syndrome (MERS)-CoV, the
67 other two highly pathogenic coronaviruses, belongs to the genus *Betacoronavirus* of the
68 *Coronaviridae* family[9]. SARS-CoV-2 is a single-strand, positive-sense, enveloped virus, with an
69 inner capsid formed by a 30-kb RNA genome wrapped by the nucleocapsid (N) proteins and a
70 lipid envelope coated with the membrane (M), envelope (E), and trimeric Spike (S) proteins[10]. The
71 S protein of SARS-CoV-2, composed of S1 and S2 subunits, is the major surface protein of the
72 virion. The S protein mediates viral entry into host cells by binding to its receptor, angiotensin-
73 converting enzyme 2 (ACE2), through the receptor-binding domain (RBD) at the C terminus of
74 the S1 subunit. This binding subsequently induces the fusion between the SARS-CoV-2 envelope
75 and the host cell membrane mediated by the S2 subunit, leading to the release of the viral genome
76 into the cytoplasm[11-14].

77 The S protein, S1 subunit, or the RBD antigen of SARS-CoV-2, could induce both B cell and T
78 cell responses, generating highly potent neutralizing antibodies against SARS-CoV-2[15-17].
79 Vaccination is the most promising approach to end COVID-19 pandemic. Traditional vaccine
80 platforms, such as inactivated, virus-like particle, and viral vector-based vaccines have been
81 adopted to develop SARS-CoV-2 vaccines[18-26]. Importantly, the mRNA vaccines against SARS-
82 CoV-2 have been developed at warp speed and urgently approved for use[27-33], even though such a
83 strategy had never been applied commercially before[34]. The mRNA vaccine contains a linear
84 single-stranded RNA, consisting of a 5' cap, the untranslated region (UTR), the antigen-coding
85 region, and a 3' polyA tail, and is delivered into the body via lipid-nano particle (LNP)
86 encapsulation[34]. The clinical-scale mRNA vaccines could be manufactured rapidly upon the viral
87 antigen sequence is released[27]. However, the current mRNA vaccine still has certain limitations,
88 including inherent instability and suboptimal thermostability after LNP encapsulation for *in vivo*
89 administration[35-37], as well as potential immunogenic side effects[38,39].

90 Circular RNAs (circRNAs) are covalently closed single-stranded RNA transcripts that comprise
91 a large class of non-coding RNAs generated in eukaryotic cells by a non-canonical RNA splicing
92 event called backsplicing in eukaryotic cells[40-42]. Some viral genomes, such as hepatitis D virus
93 and plant viroids, are circular RNAs[39]. Thousands of circRNAs have been identified in eukaryotes,
94 including fungi, plants, insects, fish, and mammals via high-throughput RNA sequencing and
95 circRNA-specific bioinformatics[42]. Unlike linear mRNA, circRNA is highly stable due to its
96 covalently closed ring structure, which protects it from exonuclease-mediated degradation[42-44]. So
97 far, only a few endogenous circRNAs have been shown to function as protein translation
98 templates[45-48]. Although circRNA lacks the essential elements for cap-dependent translation, it can
99 be engineered to enable protein translation through an internal ribosome entry site (IRES) or the
100 m6A modification incorporated to the upstream of open reading frame (ORF)[49,50].

101 Here, we attempted to develop circular RNA vaccines, aiming to provide effective protection
102 against SARS-CoV-2 and its emerging variants.

103

104 **circRNA^{RBD} produced functional SARS-CoV-2 RBD antigens**

105 We employed the Group I ribozyme autocatalysis strategy[49] to produce circular RNAs encoding
106 SARS-CoV-2 RBD antigens[29], termed circRNA^{RBD} (**Fig. 1a**). In this construct, the IRES element
107 was placed before the RBD-coding sequence to initiate its translation. To enhance the
108 immunogenicity of RBD antigens, the signal peptide sequence of human tissue plasminogen
109 activator (tPA) was fused to the N-terminus of RBD to ensure the secretion of antigens[51-53].
110 Besides, recent research reported that RBD trimmers outperformed the monomeric RBD in binding
111 hACE2[12,13,54]. To improve the immunogenicity of RBD antigens, the trimerization motif of
112 bacteriophage T4 fibritin protein (foldon)[55] was fused to its C terminus to enhance the
113 immunogenicity of RBD antigens. This IRES-SP-RBD-Foldon sequence was then cloned into the
114 vector to construct the *in vitro* transcription (IVT) template for producing circRNA^{RBD} (**Fig. 1a**).
115 The precise circularization of circRNA^{RBD} was verified by reverse transcription-PCR analysis
116 using specific primers and Sanger sequencing (**Fig. 1a**, **Extended Data Fig. 1a**, **b**).

117 Owing to its covalently closed circular structure, the circRNA^{RBD} migrated faster in
118 electrophoresis (**Extended Data Fig. 2a**) and appeared more resistant to exonuclease RNase R
119 than the linear precursor RNA (**Extended Data Fig. 2b**). High-performance liquid

120 chromatography (HPLC) showed that the RNase R treatment purged a significant amount of the
121 linear precursor RNAs, which was an important step in purifying the circRNA^{RBD} (**Extended Data**
122 **Fig. 2c**).

123 To test the secretory expression of RBD antigens produced by circRNA^{RBD}, the purified
124 circRNA^{RBD} was transfected into human HEK293T cells or murine NIH3T3 cells. Abundant RBD
125 antigens in the supernatant of both human and murine cells was detected by Western blot,
126 indicating the high compatibility of circRNAs (**Fig. 1b**). The concentration of RBD antigens
127 produced by circRNA^{RBD} reached ~1,400 ng/mL, 600-fold higher than its linear precursor RNA
128 (**Fig. 1c**).

129 Besides the Group I ribozyme autocatalysis strategy, we developed an alternative method to
130 generate circRNA^{RBD} using T4 RNA ligase (**Extended Data Fig. 3a**). Similarly, abundant RBD
131 antigens have been detected in the supernatant at a concentration of ~1,000 ng/mL concentration,
132 which is ~200-fold higher than that produced by its linear precursor RNA (**Extended Data Fig.**
133 **3b, c**).

134 To verify whether the secreted SARS-CoV-2 RBD antigens produced by circRNA^{RBD} were
135 functional, the supernatants of circRNA^{RBD}-transfected cells were used in a competition assay
136 using hACE2-overexpressing HEK293 cells (HEK293T-ACE2) and SARS-CoV-2 pseudovirus
137 harboring an EGFP reporter[56]. The secreted SARS-CoV-2 RBD antigens could effectively block
138 SARS-CoV-2 pseudovirus infection (**Fig. 1d**). Altogether, circRNA^{RBD} showed robust protein
139 expression, suggesting its potential as a novel vaccine platform.

140

141 **SARS-CoV-2 circRNA^{RBD} vaccine induced sustained humoral immune responses with high-**
142 **level of neutralizing antibodies**

143 To explore whether circRNA could be leveraged to create a new type of vaccine, we attempted to
144 assess the immunogenicity of circRNA^{RBD} encapsulated with lipid nanoparticles in BALB/c mice
145 (**Fig. 1e**). The circRNA^{RBD} encapsulation efficiency was greater than 93%, with an average
146 diameter of 100 nm (**Fig. 1f**). Mice were immunized with LNP-circRNA^{RBD} through intramuscular
147 (i.m.) injection twice at a two-week interval, at doses of 10 μg or 50 μg per mouse, with empty
148 LNP serving as the placebo (**Fig. 1g**). The amount of RBD-specific binding IgG and neutralizing

149 antibodies was measured at two- or five-weeks post the boost dose. The circRNA^{RBD} elicited high
150 level of RBD-specific IgG endpoint geometric mean titers (GMTs), reaching ~1.9×10^4 for 10 μg
151 dose and ~5.7×10^5 for 50 μg dose, indicating that circRNA^{RBD} could induce SARS-CoV-2 RBD-
152 specific antibodies (**Fig. 1h**).

153 Sera from circRNA^{RBD}-vaccinated mice could effectively neutralize both SARS-CoV-2
154 pseudovirus with 50% neutralization titer (NT50) of ~4.5×10^3 (**Extended Data Fig. 4**) and
155 authentic SARS-CoV-2 virus with NT50 of ~7.0×10^4 (**Fig. 1i**). The high level of RBD-specific
156 IgG, potent RBD antigen neutralization, and sustained SARS-CoV-2 neutralizing capacity
157 confirmed that circRNA^{RBD} vaccines induced humoral immune responses in mice.

158

159 **SARS-CoV-2 circRNA$^{RBD\text{-}Beta}$ vaccine-elicited antibodies showed preferential neutralizing**
160 **activity against Beta variant**

161 Next, we evaluated the efficacy of a circRNA$^{RBD\text{-}Beta}$, a circRNA vaccine encoding RBD/K417N-
162 E484K-N501Y antigens derived from SARS-CoV-2 Beta variant. BALB/c mice were immunized
163 with an i.m. injection of the circRNA$^{RBD\text{-}Beta}$ vaccine, followed by a boost at a two-week interval.
164 The immunized mice's sera were collected at 1 and 2 weeks post the boost. ELISA showed that
165 the RBD-Beta-specific IgG endpoint GMT was ~1.6×10^4 at two weeks post boost (**Fig. 1j**). SARS-
166 CoV-2 pseudovirus neutralization assay revealed that circRNA^{RBD}-elicited antibodies could
167 effectively neutralize all three pseudoviruses, with the highest neutralizing activity against the
168 native (D614G) strain (**Extended Data Fig. 5a**). The circRNA$^{RBD\text{-}Beta}$-elicited antibodies could
169 also neutralize all three pseudoviruses, with the highest activity against its corresponding Beta
170 variant (**Extended Data Fig. 5b**).

171 In line with pseudovirus neutralization assay, the sera from immunized mice could neutralize
172 authentic SARS-CoV-2 Beta and native (D164G) strain with NT50 of 2.6×10^4 (**Fig. 1k**) and
173 6.0×10^3 (**Fig. 1l**), respectively. Collectively, circRNA vaccine-elicited antibodies showed the
174 highest neutralizing activity against their corresponding variant strains. It's worth noting that both
175 vaccines could neutralize all three strains, albeit with varying efficacies. Nevertheless, it's likely
176 that the updated vaccines based on the mutations of the emerging variants might provide better
177 and more effective protection against SARS-CoV-2 circulating variants.

178

179 **circRNA$^{RBD\text{-}Beta}$ vaccine protected mice against the infection of Beta variant**

180 To further evaluate the protective efficacy of circRNA$^{RBD\text{-}Beta}$ vaccine *in vivo*, we employed the
181 Beta variant for authentic virus challenge experiments. Consistent with a recent report[57,58], the
182 Beta variant could infect wild-type BALB/c mice and replicate in their lungs (**Extended Data Fig.**
183 **5c**), likely due to the mutations in Spike protein such as K417N, E484Q, and N501Y[57,59]. Seven
184 weeks post the boost dose, the RBD-Beta-specific IgG endpoint GMT was still around 1.2×10^4
185 (**Extended Data Fig. 5d**), with significant neutralizing activity against RBD-Beta antigens
186 (**Extended Data Fig. 5e**). Each immunized mouse was then intranasally infected with 5×10^4 PFU
187 of Beta virus (7 weeks post the boost dose). The lung tissues were collected three days after the
188 challenge for the detection of viral RNAs. Viral loads in the lungs of vaccinated mice were
189 significantly lower compared with the placebo group (**Fig. 1m**). Consistently, only the mice in the
190 placebo group underwent weight loss (**Fig. 1n**). These results indicated that the circRNA$^{RBD\text{-}Beta}$
191 vaccine could effectively protect the mice against SARS-CoV-2 Beta.

192 Considering that the 50 μg of circRNA^{RBD} elicited a higher level of neutralizing antibodies than
193 10 μg, we postulated that the LNP delivery might have great impact on the efficacy of circular
194 RNA vaccine. After multiple tests, we were able to significantly lower the vaccine dose using one
195 of the commercial formulas (Precision Nanosystems). 10 μg of circRNA could induce neutralizing
196 antibodies at a level comparable to 50 μg (**Extended Data Fig. 6**). We thus switched our choice
197 of LNP for the rest of our experiments.

198

199 **circRNA$^{RBD\text{-}Delta}$ vaccine induced potent neutralizing antibodies against SARS-CoV-2 Delta**

200 The Delta, like the Beta variant, partially escapes the antibodies produced in the survivors or
201 vaccinees[60-62]. To develop such a variant-specific vaccine, we adopted both Group I ribozyme
202 autocatalysis and T4 RNA ligation strategies to produce circRNA$^{RBD\text{-}Delta}$. Mice were immunized
203 i.m. with 0.5 μg, 2.5 μg, 5 μg or 10 μg of circRNA$^{RBD\text{-}Delta}$ vaccines twice at a two-week interval.
204 Two weeks post the boost dose, the sera from immunized mice were collected to detect RBD-
205 specific antibodies. Vaccines of circRNA$^{RBD\text{-}Delta}$ made by either circularization methods could
206 induce high endpoint GMTs of IgG binding antibodies (**Fig. 2a**, **b**). The sera from circRNA$^{RBD\text{-}}$
207 ^{Delta}-vaccinated mice effectively neutralized the Delta pseudovirus in a dose-dependent manner,

208 with the NT50 of ~1.4×10^5 for the 10 μg dose (**Fig. 2c**).

209 Importantly, circRNA$^{RBD\text{-}Delta}$ vaccines could provide protection against other variants,
210 including the native strain, Alpha and Beta variants, albeit with varying degrees. The sera from
211 circRNA$^{RBD\text{-}Delta}$-immunized mice exhibited the highest neutralizing activity against Delta and the
212 lowest against Beta variant (**Fig. 2d**, **e**).

213

214 **circRNA vaccine enabled higher and more durable antigen expression than mRNA vaccine**

215 The circRNA is reportedly more stable than mRNA owing to its covalent closed circular
216 structure[63]. To test whether the stability of the circRNA vaccine could confer higher and more
217 durable antigen-encoding efficiency than the mRNA vaccine, we generated 1mΨ modified mRNA,
218 termed 1mΨ-mRNA, and unmodified mRNA, both of which contain the same RBD-encoding
219 sequence as the circRNA for a fair comparison. The purified circRNA, 1mΨ-mRNA, and
220 unmodified mRNA were transfected into the HEK239T cells. Cell supernatants were collected to
221 measure the abundance of RBD antigen at different time points from 12 to 96 hrs post transfection.
222 The circRNA produced much higher levels of RBD antigens at all time points and maintained for
223 longer period than both 1mΨ-mRNA and unmodified mRNA (**Fig. 3a**). The RT-qPCR showed that
224 circRNAs were more stable than mRNAs, modified or unmodified (**Fig. 3b**). Importantly, the
225 LNP-encapsulation further enhanced the advantage of circRNA in protein production and
226 durability from both 1mΨ-mRNA and unmodified-mRNA (**Fig. 3c**). Interestingly, the LNP-
227 encapsulation appeared to improve the antigen-encoding efficiency of unmodified mRNA to a
228 level comparable to 1mΨ-mRNA (**Fig. 3c**).

229 A thermostable RNA vaccine is highly desirable for efficient vaccine distribution. We found that
230 even after two weeks of storage at room temperature (~25°C), the circRNA could express RBD
231 antigens without detectable loss (**Fig. 3d**), highlighting its remarkable thermal stability. To further
232 evaluate the thermostability of vaccines, the LNP-encapsulated circRNA, 1mΨ-mRNA and
233 unmodified-mRNA were stored at 4°C, room temperature (~25°C), or 37°C for up to 28 days prior
234 to the transfection. At all temperatures tested, circRNA expressed higher levels of antigens than
235 those of the other two mRNA groups (**Extended Data Fig. 7a-c**). At 4°C, little reduction of RBD
236 antigens produced by LNP-encapsulated circRNA could be detected from 1-28 days (**Extended**
237 **Data Fig. 7a**). The stability of LNP-encapsulated circRNA, 1mΨ-mRNA and unmodified-mRNA

238 was evidently reduced with the increase of storage temperature, especially at 37°C (**Extended**
239 **Data Fig. 7b-c**). Together, although extended shelf life and high temperature deteriorate RNA-
240 based vaccines, circRNA vaccine exhibited higher stability than mRNA vaccines (**Extended Data**
241 **Fig. 7a-c**).

242

243 **circRNA vaccine elicited higher proportion of neutralizing antibodies and stronger Th1-**
244 **biased T cell immune responses than the mRNA vaccine**

245 Currently, two kinds of mRNA vaccines are widely inoculated, mRNA-1273 (Moderna) and
246 BNT162b2 (Pfizer/BioNTech), both of which contain modified 1mΨ modification. Given that
247 circRNA vaccine possesses higher stability and antigen-encoding efficiency, we wonder whether
248 it exhibited superior immunogenicity to mRNA vaccine. We first compared the balance of Th1 and
249 Th2 immune responses between circRNA$^{RBD\text{-}Delta}$ and mRNA$^{RBD\text{-}Delta}$ vaccines because Th2-biased
250 immune responses might induce vaccine-associated enhanced respiratory disease (VAERD)[27,32,64].
251 ELISA assay showed that the total IgG elicited by circRNA$^{RBD\text{-}Delta}$ was comparable to that by
252 mRNA$^{RBD\text{-}Delta}$ (**Fig. 3e**), however, the ratio of IgG2a/IgG1, IgG2c/IgG1 or (IgG2a + IgG2c)/IgG1
253 from circRNA$^{RBD\text{-}Delta}$ was higher than from mRNA$^{RBD\text{-}Delta}$ vaccine (**Fig. 3f**, **g**, **Extended Data**
254 **Fig. 8a**, **b**), indicating that circular RNA vaccines tended to induce stronger Th1-biased immune
255 responses.

256 Antibody-mediated enhancement (ADE) of infection by virus-specific antibodies is another
257 potential concern for vaccines, which has been reported for infections by some viruses including
258 Zika, Dengue virus, and coronaviruses[65-69]. Previous research has reported that the virus-binding
259 antibodies without neutralizing activity elicited by infection or vaccination possibly caused the
260 ADE effects, especially for those viruses with different serotypes[70,71]. Therefore, we compared the
261 ratio of neutralizing to binding antibodies between circRNA and mRNA vaccines. Although
262 circRNA$^{RBD\text{-}Delta}$ exhibited equal neutralizing capability compared to mRNA$^{RBD\text{-}Delta}$ (**Fig. 3h-j**),
263 the former induced a higher proportion of neutralizing antibodies at all doses tested (0.5 μg, 2.5
264 μg, and 5 μg) in mice (**Fig. 3k**). Owing to this unique feature, the circRNA vaccine might have
265 certain advantage to circumvent potential ADE effects and tolerate viral mutations.

266

267 **circRNA$^{RBD\text{-}Delta}$ vaccine elicited strong T cell immune responses**

268 B cells, CD4$^+$ T cells, and CD8$^+$ T cells are three pillars of adaptive immunity. They mediated
269 effector functions against SARS-CoV-2 in both non-hospitalized and hospitalized cases of
270 COVID-19[72].

271 To compare CD4$^+$ and CD8$^+$ T cell immune responses, the splenocytes of immunized mice were
272 collected and stimulated with SARS-CoV-2 RBD-Delta pooled peptides (**Supplementary Table**
273 **1**), and cytokine-producing T cells were quantified by intracellular cytokine staining among
274 effector memory T cells (Tem, CD44$^+$CD62L$^-$) (**Extended Data Fig. 9**). Stimulated with RBD-
275 Delta peptide pools, CD8$^+$ T cells producing interferon-γ (IFN-γ), tumor necrosis factor (TNF-α),
276 and interleukin-2 (IL-2) were detected in mice immunized with circRNA$^{RBD\text{-}Delta}$ vaccine or
277 1mΨU-mRNA$^{RBD\text{-}Delta}$ vaccine (**Extended Data Fig. 10a-c**), indicating the RBD-specific CD8$^+$ T
278 cell responses elicited by both vaccines. The CD4$^+$ T cells of immunized mice induced strong IFN-
279 γ, TNF-α, and IL-2 responses, but minimal IL-4 responses (**Extended Data Fig. 10d-g**), indicating
280 that both circRNA$^{RBD\text{-}Delta}$ and 1mΨ-mRNA$^{RBD\text{-}Delta}$ induced the Th1-biased T cell immune
281 responses (**Extended Data Fig. 10d-g**).

282

283 **circRNA$^{RBD\text{-}Delta}$ vaccine elicited high level of broad-spectrum neutralizing antibodies against**
284 **both Delta and Omicron variants**

285 The emerging SARS-CoV-2 Omicron variant contains more than 30 mutations in the Spike region
286 and spreads quickly[3]. It has been reported that the Omicron variant escaped most of the previously
287 reported neutralizing antibodies and the sera of vaccinees who received two-dose original SARS-
288 CoV-2 vaccines[4-8]. To cope with this emergency, we tested the neutralizing capability elicited by
289 all three circRNA vaccines against Omicron variant. The neutralizing activity against Omicron
290 from the sera of mice immunized with either one of the three vaccines dropped 74-fold (native),
291 15-fold (Beta) and 44-fold (Delta) in comparison with against their corresponding variants (**Fig.**
292 **4a**). Among all three, circRNA$^{RBD\text{-}Delta}$ vaccine maintained sufficient neutralizing activity against
293 Omicron (**Fig. 4a**), with the NT50 of ~4.7×10^3, while the NT50 of the circRNA$^{RBD\text{-}Beta}$ against
294 Omicron dropped to below 5×10^2 (**Fig. 4a**). Compared to mRNA$^{RBD\text{-}Delta}$ vaccine, circRNA$^{RBD\text{-}}$
295 ^{Delta} vaccine elicited comparable neutralizing activity against both Delta and Omicron variants for
296 mouse sera collected at 2 weeks post boost (short-term) and 7 weeks post boost (long-term) (**Fig.**

297 **4a-c**). Similar to the above observations (**Fig. 3h-k**), circRNA$^{RBD-Delta}$ vaccine also elicited higher
298 proportion of neutralizing antibodies against Omicron variant than 1mΨ-mRNA$^{RBD-Delta}$ vaccine at
299 both 2 weeks post boost (short-term) and 7 weeks post boost (long-term) (**Extended Data Fig.**
300 **11a-d**), indicating the potential superiority of circRNA vaccine against the circulating variants of
301 SARS-CoV-2, likely owing to its high proportion of neutralizing antibody (**Fig. 3h-k** and
302 **Extended Data Fig. 11a-d**).

303

304 **circRNA$^{RBD-Omicron}$ vaccine elicited neutralizing antibodies against Omicron**

305 We have developed Omicron-specific circRNA vaccine, which expressed the trimeric RBD
306 antigens of Omicron variant. Mice were immunized i.m. with 5 μg or 10 μg of circRNA$^{RBD-Omicron}$
307 vaccines twice at a 2-week interval. One week post the boost dose, the serum samples from
308 immunized mice were collected for the detection of Omicron-specific antibodies. The
309 circRNA$^{RBD-Omicron}$ vaccine could induce Omicron Spike-specific antibodies with the endpoint
310 GMTs of ~4.7×10^4 for 5 μg dose and ~2.2×10^5 for 10 μg dose (**Fig. 4d**), yielding evident
311 neutralizing activities against Omicron with the NT50 of ~2.5×10^3 for the 5 μg dose and ~8.6×10^3
312 for the 10 μg dose (**Fig. 4e**). However, neutralizing activity could hardly be detected against native
313 strain or Delta variant (**Fig. 4e, f**).

314

315 **The third booster with circRNA$^{RBD-Delta}$ vaccine remarkably elevated the neutralizing**
316 **antibodies against current VOC of SARS-CoV-2**

317 We next investigated the feasibility of circRNA vaccine as a booster for the protection against
318 Omicron variant. Mice immunized with two doses of circRNA$^{RBD-Delta}$ vaccines received the 3rd
319 booster with circRNA$^{RBD-Beta}$, circRNA$^{RBD-Delta}$ or circRNA$^{RBD-Omicron}$ vaccine at 7 weeks post the
320 2nd dose, followed by the assessment of neutralizing activity against the Omicron variant at 1 week
321 post the 3rd boost (**Fig. 4g**). Only circRNA$^{RBD-Delta}$ effectively boosted the neutralizing antibodies
322 against both Delta (**Fig. 4h**) and Omicron (**Fig. 4i**). On the contrary, the 3rd boost with the
323 circRNA$^{RBD-Beta}$ or circRNA$^{RBD-Omicron}$ vaccine failed to elevate the neutralizing capability against
324 Omicron (**Fig. 4h, i**).

325 We then went on to test the 3rd booster with circRNA^{RBD} or circRNA$^{RBD-Delta}$ vaccine on mice

326 previously immunized with 2 doses of circRNA^{RBD} vaccines (**Fig. 4j**). Both vaccines could
327 effectively boost the neutralizing antibodies against both Delta (**Fig. 4k**) and Omicron (**Fig. 4l**).
328 circRNA$^{RBD\text{-}Delta}$ appeared to be a much better booster than circRNA^{RBD} against both Delta and
329 Omicron variants, which elevated the geometric mean NT50 from ~4×10^2 to ~3.2×10^4 against
330 Omicron variant (**Fig. 4k**, **l**).

331 Taken together, these results suggest that circRNA$^{RBD\text{-}Delta}$ might be a favorable choice for
332 vaccination to provide a broad-spectrum protection against the current VOC of SARS-CoV-2.
333 However, the 3rd booster with Omicron-specific vaccines might not be an appropriate strategy
334 against the current Delta and Omicron emergency in the real world.

335

336 **circRNA vaccine elicited potent neutralizing antibodies and Th1-biased immune responses**
337 **in rhesus macaques**

338 To further assess the immunogenicity of circRNA vaccine in non-human primates (NHPs), groups
339 of 2~4-year-old rhesus macaques were immunized i.m. with 20 μg, 100 μg or 500 μg of
340 circRNA^{RBD} vaccines, 100 μg of circRNA^{Ctrl}, or PBS control on Days 0 and 21 (**Fig. 5a**). The total
341 RBD-specific IgG binding and neutralizing antibodies were measured using the plasma of rhesus
342 macaques at two weeks post the boost dose (**Fig. 5a**). The IgG endpoint GMTs reached ~2.1×10^4
343 (20 μg), ~1.6×10^4 (100 μg dose) and ~7×10^3 (500 μg dose) for circRNA^{RBD} vaccines, while
344 circRNA^{Ctrl} or PBS-immunized rhesus macaques failed to induce RBD-specific antibodies (**Fig.**
345 **5b**). The SARS-CoV-2 pseudovirus neutralization assay showed the NT50 of ~180 for 20 μg dose,
346 ~520 for 100 μg dose, and ~390 for 500 μg dose (**Fig. 5c**). The authentic SARS-CoV-2
347 neutralization assay showed the NT50 of ~80 for 20 μg dose, ~120 for 100 μg dose, and ~50 for
348 500 μg dose (**Fig. 5d**, **e**). These results indicated that the 100 μg dose could elicit maximal level
349 of neutralizing antibodies (**Fig. 5c**, **d**).

350 We then performed the cross-neutralizing assay using the plasma samples from the immunized
351 rhesus macaques. Both the pseudotyped and authentic SARS-CoV-2 neutralization assay showed
352 that the circRNA^{RBD} vaccine-immunized rhesus macaque plasma could effectively inhibit the
353 corresponding native strain, while Alpha, Delta and Beta variants could also be inhibited, but with
354 reduced activity, especially for the Beta variant (**Fig. 5d**, **e**).

355 The peripheral blood mononuclear cells (PBMCs) collected on the day before challenge with
356 SARS-CoV-2. The RBD-specific T cell responses elicited by circRNA^{RBD} vaccines or controls in
357 rhesus macaques were measured using the PBMCs stimulated with the corresponding RBD peptide
358 pools (**Supplementary Table 2**). ELISpot assay showed evident IFN-γ and IL-2 responses, but
359 nearly undetectable IL-4 in circRNA^{RBD}-immunized rhesus macaques (**Fig. 5f**), indicating a Th1-
360 biased T cell immune response.
361

362 **circRNA vaccine protected the rhesus macaques against SARS-CoV-2 infection**

363 Five weeks post the boost dose, the immunized rhesus macaques were challenged with 1×10^6
364 plaque forming units of SARS-CoV-2 native strain via intranasal and intratracheal routes, as
365 described previously[33]. The challenged rhesus macaques were euthanized at 7 dpi, and the lung
366 tissues were underwent viral load and histopathological assays. The RT-qPCR assay using primers
367 targeting SARS-CoV-2 genomic RNA (N protein region) indicated that the rhesus macaques
368 immunized with 100 μg or 500 μg of circRNA^{RBD} vaccine were well protected as the viral genomic
369 RNA copies were reduced nearly 1000-fold compared to the control groups (**Fig. 5g**). To detect
370 the actively replicative viral loads, we performed qPCR using primers targeting SARS-CoV-2 sub-
371 genomic RNA (E protein region), and found that circRNA^{RBD}-immunized rhesus macaques of all
372 three doses had nearly no detectable viral sub-genomic RNA in the lung tissues (**Fig. 5g**).
373 Further histopathological examination demonstrated that circRNA^{RBD}-immunized rhesus
374 macaques of all doses were well protected because only very mild pneumonia was observed,
375 especially in the two high-dose groups (**Fig. 5h**). In contrast, severe pneumonia symptoms were
376 observed in the lungs of two control groups, as exemplified by the local pulmonary septal
377 thickening, moderate hemorrhage in the pulmonary septals, a large number of scattered dust cells,
378 and massive inflammation cells infiltration (**Fig. 5h**). Pathological score further confirmed that
379 circRNA^{RBD} immunization significantly protected the rhesus macaques from SARS-CoV-2
380 infection (**Fig. 5i**), likely resulting from a synergy between the humoral immune responses and T
381 cell responses elicited by vaccination (**Fig. 5j**).
382

383 **circRNA vaccine did not cause clinical signs of illness in rhesus macaques**

384 To further evaluate the immunogenicity and safety of circRNA vaccines in NHP, physiological

385 and biochemical indicators were monitored, including adverse effects, cytokines indicating innate
386 immune activation, body weight, body temperature, and blood routine examination. No severe
387 clinical adverse effects were observed following the priming dose or the 2nd boost. ELISA results
388 showed that circRNA^{RBD} vaccines induced high levels of IL-6 and MCP-1 (**Extended Data Fig.**
389 **12a, b**), while the TNF-α, IL-1β, and IFN-α were nearly undetectable (**Extended Data Fig. 12c-**
390 **e**). Body temperatures of both immunized rhesus macaques and controls were within the normal
391 range, which have been continuously monitored for 3 days after prime and boost (**Extended Data**
392 **Fig. 12f**). None of the challenged macaques showed clinical signs of illness (**Extended Data Fig.**
393 **13a-e**). Collectively, our study provided preliminary proof of safety for the circRNA vaccination
394 in NHPs.

395

396 **Expression of SARS-CoV-2 neutralizing antibodies via circRNA platform**

397 Besides vaccine, circRNA could be re-purposed for therapeutics when used to express other
398 proteins or peptides, such as enzymes for rare diseases and antibodies for infectious diseases or
399 cancer. Here, we attempted to test the therapeutic potential of circRNAs by expressing the SARS-
400 CoV-2 neutralizing antibodies. It has been reported that SARS-CoV-2 neutralizing nanobodies or
401 hACE2 decoys could inhibit the SARS-CoV-2 infection[73-75]. This prompted us to leverage the
402 circRNA platform to express SARS-CoV-2 neutralizing nanobodies, including nAB1, nAB1-Tri,
403 nAB2, nAB2-Tri, nAB3, and nAB3-Tri[73,74], together with hACE2 decoys[75] (**Extended Data Fig.**
404 **14a**). Pseudovirus neutralization assay showed that supernatants of HEK293T cells transfected
405 with circRNA^{nAB} or circRNA$^{hACE2\ decoys}$ could effectively inhibit wild SARS-CoV-2 S-protein
406 based pseudovirus infection (**Extended Data Fig. 14b**).

407 Next, we tested neutralizing antibodies against the recently emerged SARS-CoV-2 variants,
408 including Alpha variant and Beta variant, by pseudovirus assays. Consistent with other reports[73,74],
409 the supernatants of circRNA$^{nAB1\text{-}Tri}$ and circRNA$^{nAB3\text{-}Tri}$ transfected cells effectively blocked Alpha
410 and D614G pseudovirus infection (**Extended Data Fig. 14c**). However, both nanobodies showed
411 markedly decreased neutralizing activity against Beta variant (**Extended Data Fig. 14c**). The
412 hACE2 decoys showed no inhibition activity against Alpha and Beta variants (**Extended Data Fig.**
413 **14c**).

414

415 **Discussion**

416 COVID-19 is still a fast-growing global health crisis with circulating SAS-CoV-2 variants evading
417 immunity from prior vaccination or viral infection, especially with the emerging Delta and
418 Omicron variants of concern[76-79]. The Omicron variant has been reported to escape most of SARS-
419 CoV-2 neutralizing antibodies and the sera from vaccinees or convalescent patients[4-8]. Our study
420 established a circular RNA vaccination strategy to elicit effective neutralizing antibodies and T
421 cell immune responses against SARS-CoV-2 and its emerging variants (**Fig. 4** and **Fig. 5)**.

422 As reported, most effective neutralizing antibodies recognize the RBD region of Spike
423 protein[73,74,80-83], and targeting RBD may induce fewer non-neutralizing antibodies[29-32,84]. Given
424 that RBD trimers bind hACE2 better than monomeric counterparts[54] and have been shown to
425 enhance humoral immune response[32,54,85], we chose to express RBD trimers via circRNA as the
426 immunogen. The circRNA-encoded RBD trimmers were functional (**Fig. 1d**) and indeed induced
427 sustained high-level neutralizing antibodies and specific T cell immune responses against SARS-
428 CoV-2 and variants in both mice and rhesus macaques (**Fig. 2**, **Fig. 5** and **Extended Data Fig. 10**).

429 The mRNA vaccines based on the full-length Spike protein (mRNA-1273 and BNT162b2)[27,28,33]
430 or RBD elicit neutralizing antibodies and T cells immune responses[29-32,84]. In comparison with the
431 mRNA vaccine, circRNA vaccine elicited longer-lasting and higher level of immunogens (**Fig.**
432 **3a-d** and **Extended Data Fig. 7**), leading to stronger Th1-biased T cell immune responses (**Fig.**
433 **3e-g**, **Extended Data Fig. 8**), suggesting that circular RNA vaccine might have a better chance to
434 avoid the vaccine-associated enhanced respiratory disease (VAERD)[27,32,64]. Moreover,
435 circRNA$^{\text{RBD-Delta}}$ vaccine induced higher proportion of neutralizing antibodies against both Delta
436 and Omicron variants than mRNA$^{\text{RBD-Delta}}$ vaccine (**Fig. 3h-k** and **Extended Data Fig. 11**),
437 suggesting that the circRNA vaccine platform might have superiority to cope with the potential
438 ADE effects and emerging variants[65,66].

439 It's worthy of note that the mRNA vaccine we used for the comparison study is different from
440 the two widely inoculated vaccines, mRNA-1273 and BNT162b2, both of which encode the full-
441 length Spike antigens and were produced by different manufacturing process[27,28,33].

442 Recently, Omicron variant rose rapidly, accounting for ~30% of total COVID-19 cases
443 worldwide as of Dec. 28, 2021 (GISAID). Omicron has been reported to escape most neutralizing
444 antibodies and the inhibition from convalescent sera[4-8]. The fact that circRNA$^{\text{RBD-Omicron}}$ vaccine

445 we developed could not cross-protect Delta variant (**Fig. 4d-f**) suggests that the immunogenicity
446 of Omicron RBD was less effective and largely different from Delta RBD[3].

447 A recent preprint reported that vaccinees who received two doses of SARS-CoV-2 vaccine
448 exhibited enhanced neutralizing antibodies against Delta variant after infected by Omicron,
449 implying that Omicron vaccine might provide broad-spectrum protection against other variants[86].
450 Our result argues against such possibility because our Omicron-specific vaccine failed to cross
451 protect Delta variant (**Fig. 4d-f**), or boost two-dose of Delta vaccine (**Fig. 4h, i**). On the contrary,
452 circRNA$^{\text{RBD-Delta}}$ vaccine appeared to produce antigens possessing high immunogenicity and
453 consequently elicit high level of neutralizing antibodies against Delta (**Fig. 2**). Our Delta-specific
454 vaccination could cross protect all other variants including Omicron (**Fig. 2** and **Fig. 4a-c**), and it
455 could also be used as an effective booster following two-dose original SARS-CoV-2 vaccines (**Fig.**
456 **4k, l**). It is hopeful but remains to be further tested whether circRNA$^{\text{RBD-Delta}}$ vaccine could be
457 applied as an effective booster for current major vaccines, which are exclusively based on the
458 original SARS-CoV-2 strain.

459 It has been a concerning issue whether the circRNAs produced via *in vitro* transcription induce
460 strong innate immune responses[38,39,87]. Our vaccination study in rhesus macaques demonstrated
461 that circRNA vaccine could indeed provide safe protection against SARS-CoV-2 infection without
462 causing severe clinical signs of illness (**Fig. 5**, **Extended Data Fig. 12a-f** and **Extended Data Fig.**
463 **13a-e**).

464 In this study, we also tested the therapeutic potential of circRNAs that encode SARS-CoV-2-
465 specific neutralizing nanobodies[73,74,80-83] or hACE2 decoys[88,89], which could effectively neutralize
466 the SARS-CoV-2 pseudovirus **(Extended Data Fig. 14a-c)**. Beyond viral receptors, this circRNA
467 expression platform hold the potential to become therapeutic drugs, encoding therapeutic
468 antibodies *in vivo,* such as anti-PD1/PD-L1 antibodies[90,91]. Unlike antibodies and protein drugs,
469 circRNAs encode therapeutic antibodies in the cytoplasm, allowing them to target intracellular
470 targets like TP53[92] and KRAS[93], bypassing the cytomembrane barrier.

471 Collectively, circular RNA holds the potential to become an effective and safe vaccine platform
472 against viral infection, including SARS-CoV-2 emerging variants, as well as a therapeutic platform,
473 owing to its specific properties.

474

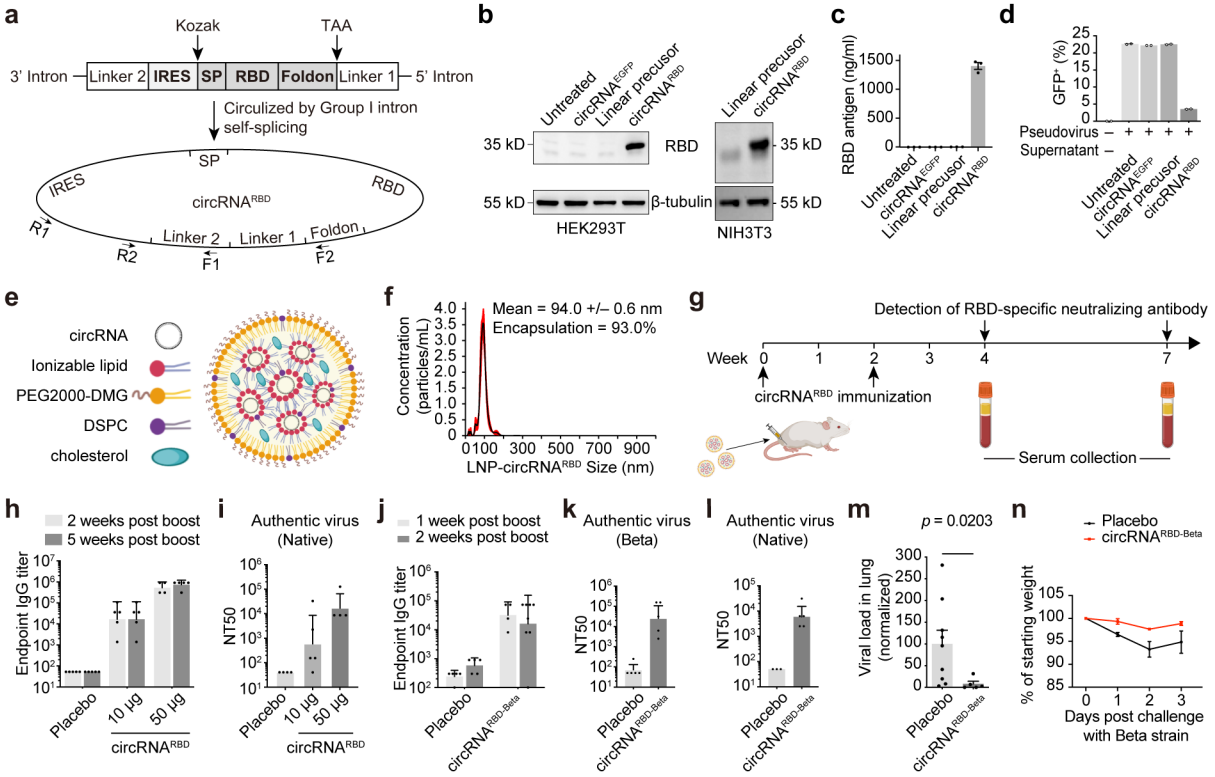

Fig. 1 | Immunogenicity and protection of circRNA vaccines against SARS-CoV-2 in mice. a, Schematic diagram of circRNA^{RBD} circularization by the Group I ribozyme autocatalysis. SP, signal peptide sequence of human tPA protein. Foldon, the trimerization domain from bacteriophage T4 fibritin protein. RBD, the receptor binding domain of SARS-CoV-2 Spike protein. The arrows indicate the design of primers for PCR analysis. **b**, Western Blot analysis showing the expression level of RBD antigens in the supernatant of HEK293T or NIH3T3 cells transfected with circRNA^{RBD} circularization by the Group I ribozyme autocatalysis. The circRNA^{EGFP} and linear RNA precursor were set as controls. **c**, Quantitative ELISA assay to measure the concentration of RBD antigens in the supernatant of HEK293T cells. **d**, Quantification of the competitive inhibition of SARS-CoV-2 pseudovirus infection (EGFP) by the circRNA^{RBD}-translated RBD antigens in the supernatant of HEK293T cells. The circRNA^{EGFP} and linear RNA precursor were set as controls. In **c** and **d**, data were shown as the mean ± S.E.M. (n = 2 or 3). **e**, Schematic representation of LNP-circRNA complex. **f**, Representative of concentration-size graph of LNP-circRNA^{RBD} measured by dynamic light scattering method. **g**, Schematic diagram of the circRNA^{RBD} vaccination process in BALB/c mice and serum collection schedule for specific antibodies analysis. **h**, Measuring the SARS-CoV-2 specific IgG antibody endpoint GMTs elicited by circRNA^{RBD} vaccine with ELISA. **i**, Neutralization assay of SARS-CoV-2 authentic virus with

493 the sera of mice immunized with circRNA^{RBD} vaccines. The serum samples were collected at 5
494 weeks post boost. **j**, Measuring the SARS-CoV-2 (Beta) specific IgG antibody endpoint GMTs
495 elicited by circRNA$^{RBD\text{-}Beta}$ vaccine with ELISA. **k**, Neutralization assay of SARS-CoV-2 (Beta)
496 authentic virus with the serum of mice immunized with circRNA$^{RBD\text{-}Beta}$ vaccines. **l**, Neutralization
497 assay of SARS-CoV-2 (D614G) authentic virus with the serum of mice immunized with
498 circRNA$^{RBD\text{-}Beta}$ vaccines. In **h** and **l**, data were shown as the geometric mean ± geometric S.D.,
499 and each symbol represented an individual mouse. **m**, Viral loads in the lung tissues of mice
500 challenged with authentic SARS-CoV-2 Beta. In **m**, data were shown as the mean ± S.E.M. (n >=
501 5), and the statistical test was performed by unpaired two-sided Student's *t*-test. **n**, The weight
502 change of immunized or placebo mice after SARS-CoV-2 Beta challenge. In **n**, data were shown
503 as the mean ± S.E.M. (n >= 5).
504
505

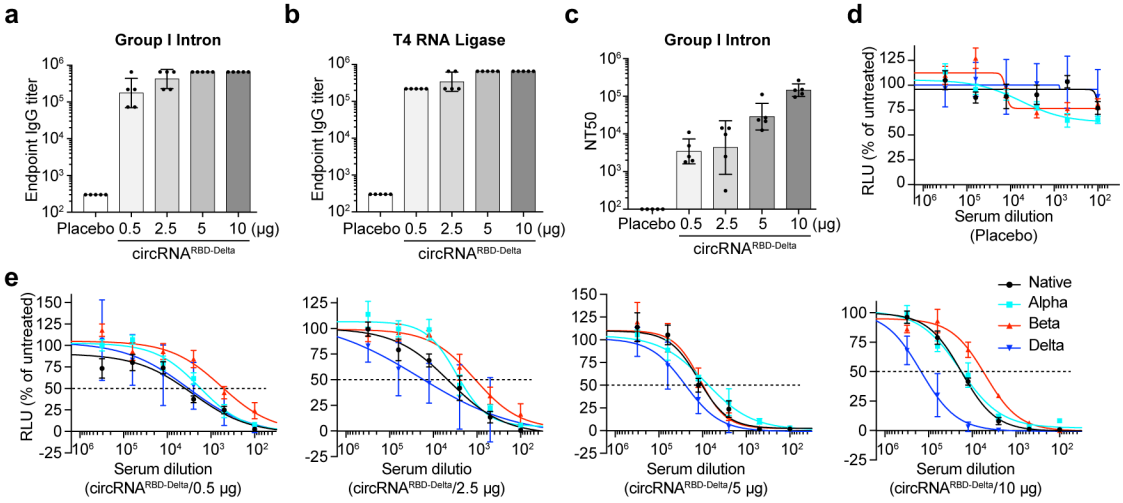

Fig. 2 | Humoral immune responses elicited by circRNA$^{\text{RBD-Delta}}$ vaccines in mice. a, Measuring the SARS-CoV-2 Delta specific IgG antibody endpoint GMTs of circRNA$^{\text{RBD-Delta}}$ vaccines generated by Group I ribozyme autocatalysis with ELISA. The data were shown as the mean ± S.E.M. (n = 5). **b**, Measuring the SARS-CoV-2 Delta specific IgG antibody endpoint GMTs of circRNA$^{\text{RBD-Delta}}$ vaccines generated by T4 RNA ligase with ELISA. The data were shown as the mean ± S.E.M. (n = 5). **c**, Neutralization assay of VSV-based SARS-CoV-2 (Delta) pseudovirus with the sera of mice immunized with circRNA$^{\text{RBD-Delta}}$ vaccines. The data were shown as the mean ± S.E.M. (n = 5). In **a-c**, data were shown as the geometric mean ± geometric S.D., and each symbol represented an individual mouse. **d** and **e**, Neutralization assay of SARS-CoV-2 native, Alpha, Beta and Delta pseudovirus with the sera of mice immunized with placebo control (**d**), or 0.5 μg, 2.5 μg, 5 μg, or 10 μg of circRNA$^{\text{RBD-Delta}}$ vaccines (**e**). In **d** and **e**, data were shown as the mean ± S.E.M. (n >= 5). In **a-e,** the serum samples were collected at 2 weeks post boost.

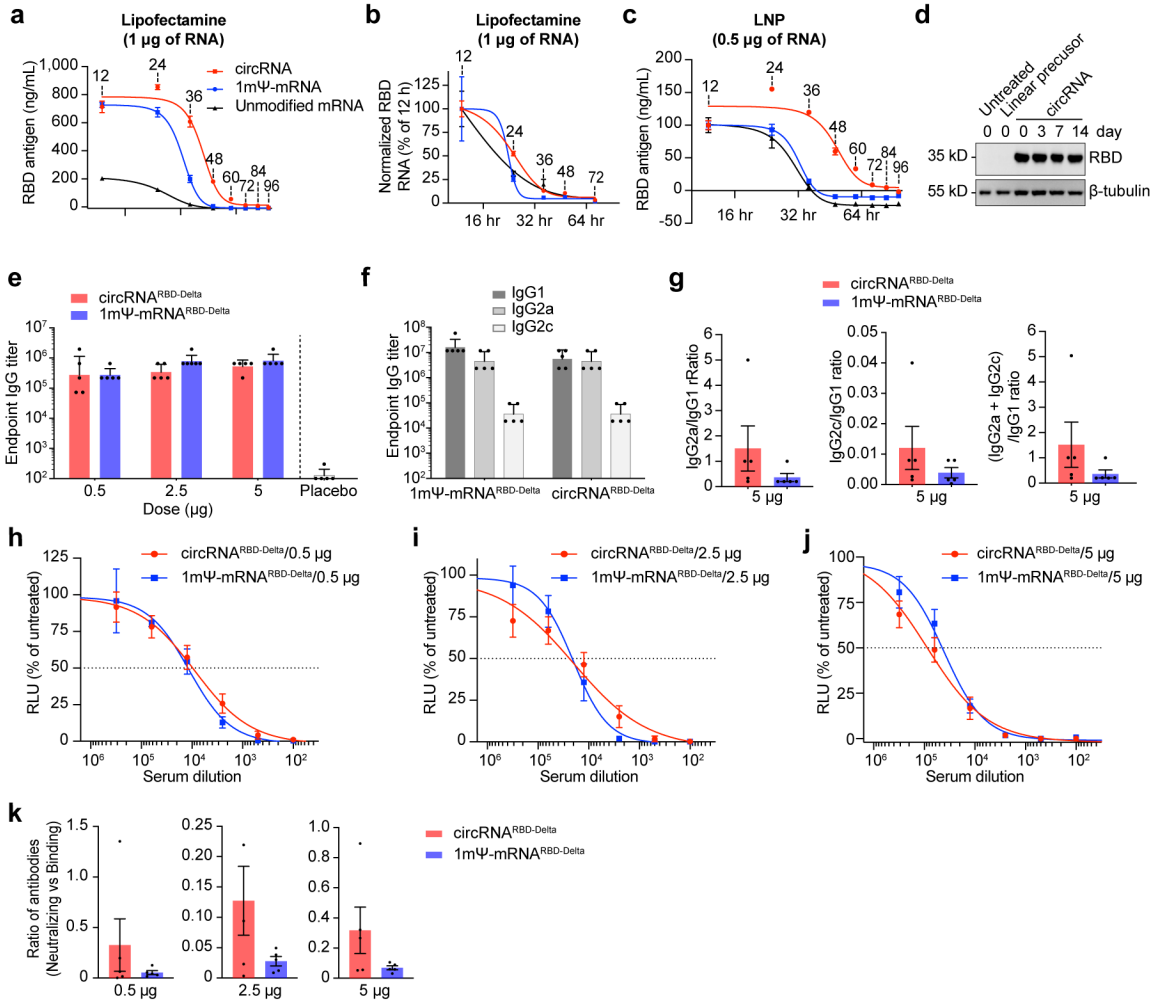

Fig. 3 | circRNA vaccine elicited higher proportion of neutralizing antibodies and stronger Th1-biased T cell immune responses than mRNA vaccine. a, Comparing antigen expression level of circRNA$^{RBD\text{-}Delta}$, 1mΨ-mRNA$^{RBD\text{-}Delta}$ and non-modified mRNA$^{RBD\text{-}Delta}$ through lipofectamine transfection in HEK293T cells by ELISA at different time points. **b**, The dynamic change of RNA level in (**a**). **c**, Comparing antigen expression level of LNP-circRNA, LNP-1mΨ-mRNA or LNP-non-modified-mRNA delivered into HEK293T cells with ELISA at indicated time points. In **a-c**, data were shown as the mean ± S.E.M. (n = 3). The data were shown as the mean ± S.E.M. (n = 3). **d**, Western Blot analysis showing the expression level of RBD antigens in the supernatant of HEK293T cells transfected with circRNA^{RBD}. The circRNA^{RBD} were stored at room temperature and transfected in days 0, 3, 7 and 14. The untreated and linear precursor were used as controls. **e**, Measuring the RBD-Delta-specific IgG endpoint GMTs elicited by circRNA^{RBD} vaccine or mRNA vaccine. The data were shown as the mean ± S.E.M. (n = 5). **f**, Measuring RBD-Delta-specific IgG1/IgG2a/IgG2c endpoint GMTs elicited by 5 μg of circRNA^{RBD} vaccine or

535 mRNA vaccine in mice. In **e** and **f**, data were shown as the geometric mean ± geometric S.D., and
536 each symbol represented an individual mouse. **g**, Measuring the specific IgG2a/IgG1, IgG2c/IgG1
537 and (IgG2a + IgG2c)/IgG1 ratio of serum from mice immunized with 5 μg of circRNA$^{RBD\text{-}Delta}$ or
538 mRNA$^{RBD\text{-}Delta}$. **h-j**, Sigmoidal curve diagram of neutralization rate of VSV-based SARS-CoV-2
539 (Delta) pseudovirus with the sera from mice immunized with different dose of circRNA$^{RBD\text{-}Delta}$ or
540 mRNA$^{RBD\text{-}Delta}$ vaccines. The serum samples were collected at 2 weeks post boost. **k**, Measuring
541 the ratio of (Neutralizing antibodies)/(Binding antibodies) elicited by circRNA$^{RBD\text{-}Delta}$ or
542 mRNA$^{RBD\text{-}Delta}$ vaccine. The ratio of (NT50)/(Endpoint GMT) of each mouse was calculated. In **g-**
543 **k**, data were shown as the mean ± S.E.M. (n >= 4) and each symbol represented an individual
544 mouse.
545
546

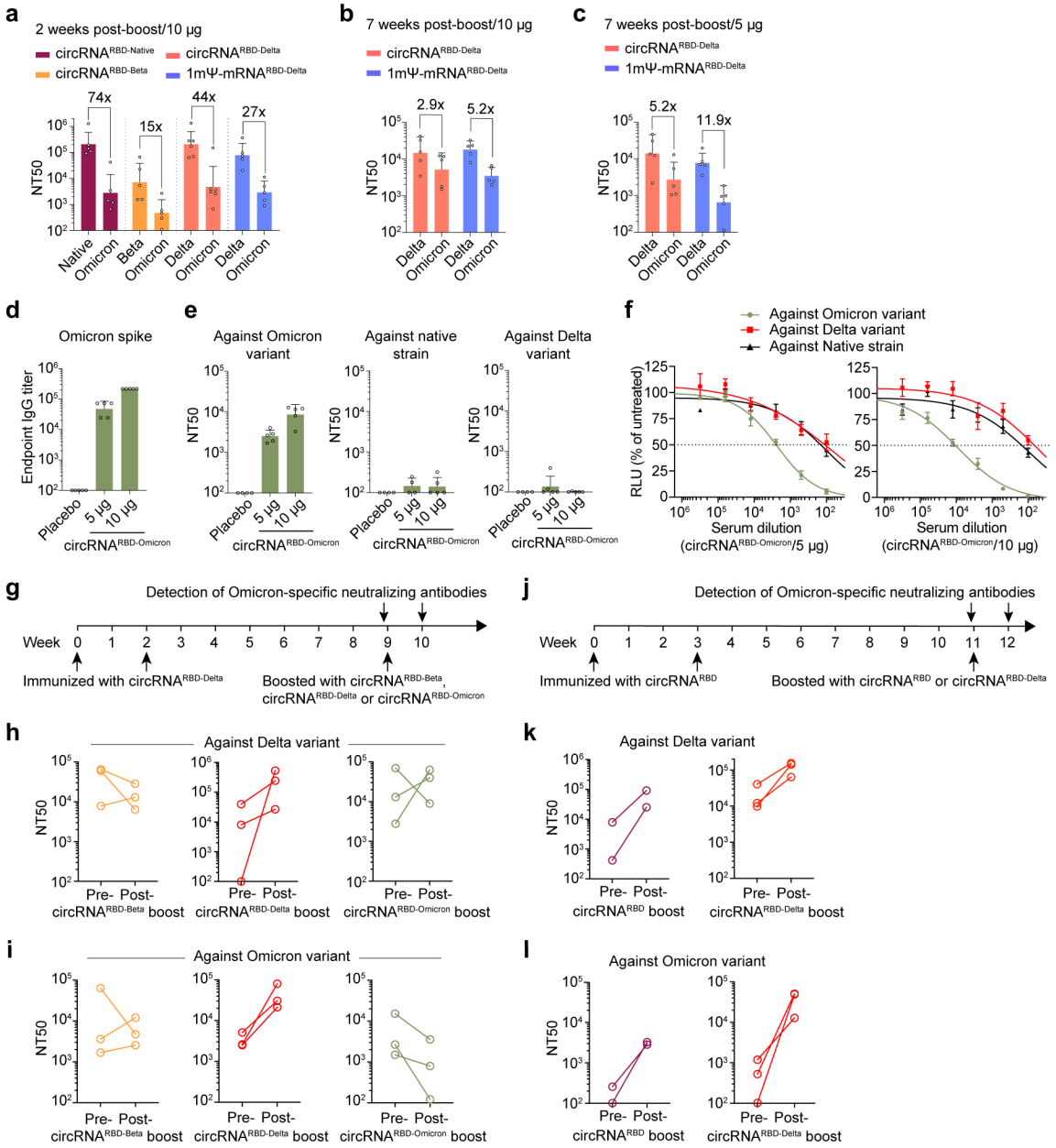

Fig. 4 | circRNA$^{\text{RBD-Delta}}$ vaccine elicited high-level of neutralizing antibodies against both Delta and Omicron variants. a, Neutralization assay of VSV-based SARS-CoV-2 pseudovirus with the sera of mice immunized with 10 μg of circRNA^{RBD}, circRNA$^{\text{RBD-Beta}}$, circRNA$^{\text{RBD-Delta}}$ or mRNA$^{\text{RBD-Delta}}$ vaccines. The serum samples were collected at two weeks post boost. **b** and **c**, Neutralization assay of VSV-based SARS-CoV-2 pseudovirus with the sera of mice immunized with 10 μg (**b**) or 5 μg (**c**) of circRNA$^{\text{RBD-Delta}}$ or mRNA$^{\text{RBD-Delta}}$ vaccines. The serum samples were collected at 7 weeks post boost. **d**, Measuring the Omicron-Spike-specific IgG endpoint GMTs of circRNA$^{\text{RBD-Omicron}}$-immunized mouse sera with ELISA. **e**, Measuring the NT50 of LNP-

556 circRNA$^{RBD\text{-}Omicron}$-immunized mouse sera using VSV-based pseudovirus of Omicron, Delta and
557 native strain. The serum samples were collected at 1 week post boost dose. In **a-e**, data were shown
558 as the geometric mean ± geometric S.D., and each symbol represented an individual mouse. **f**,
559 Sigmoidal curve diagram of the neutralization assay using VSV-based pseudovirus of Omicron,
560 Delta and native strain with the sera of mice immunized with 5 μg or 10 μg of circRNA$^{RBD\text{-}Omicron}$
561 vaccines. In **f**, the serum samples were collected at 1 week post boost, and data were shown as the
562 mean ± S.E.M. (n = 4 or 5). g, Schematic diagram of circRNA vaccination process in BALB/c
563 mice and serum collection schedule for detecting specific neutralizing antibodies. **h** and **i**,
564 Measuring the NT50 value of 5 μg of circRNA$^{RBD\text{-}Beta}$, circRNA$^{RBD\text{-}Delta}$ or circRNA$^{RBD\text{-}Omicron}$-
565 boosted mouse sera after receiving two-dose circRNA$^{RBD\text{-}Delta}$ vaccine (5 μg) using VSV-based
566 pseudovirus of Delta (**h**) or Omicron (**i**). In **h** and **i**, each symbol represented an individual mouse.
567 **j**, Schematic diagram of the LNP-circRNA vaccination process in BALB/c mice and serum
568 collection schedule for specific antibodies analysis. **k** and **l**, Measuring the NT50 value of mouse
569 sera boosted with 20 μg of circRNA^{RBD} or circRNA$^{RBD\text{-}Delta}$ vaccine after receiving two-dose
570 circRNA^{RBD} vaccine (20 μg) using VSV-based pseudovirus of Delta (**k**) or Omicron (**l**). In **k** and
571 **l**, each symbol represented an individual mouse.
572
573
574

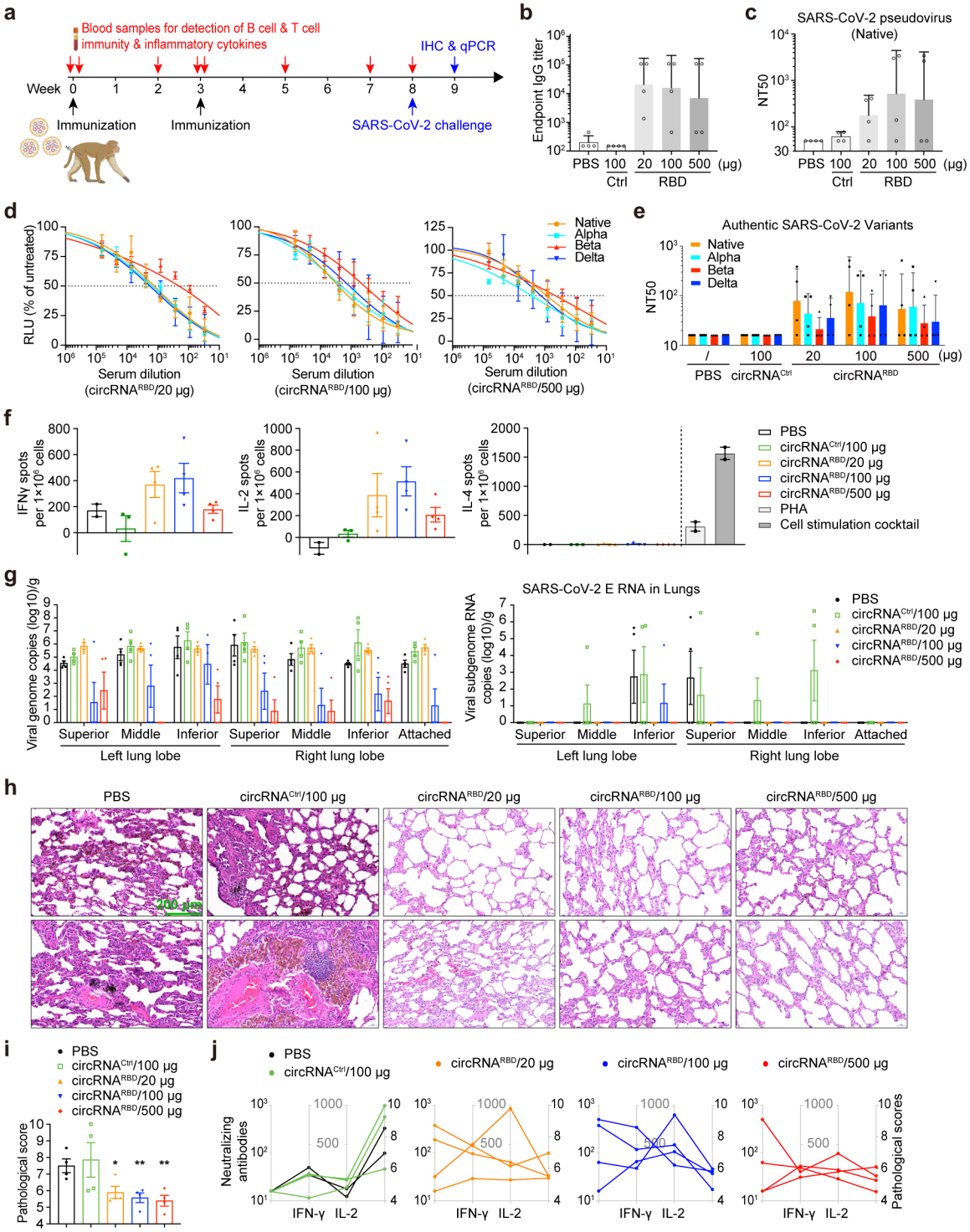

575

576 **Fig. 5 | circRNA vaccine-elicited immunogenicity and protection against SARS-CoV-2**
577 **infection in rhesus macaques. a**, Schematic diagram of the circRNA^{RBD} vaccination process in
578 rhesus macaques and plasma collection schedule for specific antibodies analysis. **b**, Measuring the
579 SARS-CoV-2 RBD-specific IgG endpoint GMTs of the plasma from the rhesus macaques

580 immunized with circRNA^{RBD} vaccine, or circRNA^{Ctrl} (circRNA without the RBD-encoding
581 sequence) or PBS controls using ELISA assay. The data were shown as the mean ± S.E.M. (n =
582 4). **c**, Measuring the NT50 of the plasma from the rhesus macaques immunized with circRNA^{RBD}
583 vaccine with ELISA using VSV-based SARS-CoV-2 pseudovirus. In **b** and **c**, data were shown as
584 the geometric mean ± geometric S.D., and each symbol represented an individual mouse. **d**,
585 Sigmoidal curve diagram of neutralization rate of VSV-based SARS-CoV-2 native, Alpha, Beta
586 and Delta pseudovirus using the plasma from the rhesus macaques immunized with circRNA^{RBD}
587 vaccine. The data were shown as the mean ± S.E.M. (n = 4), and each symbol represented an
588 individual rhesus macaque. **e**. Neutralization assay of authentic SARS-CoV-2 native, Alpha, Beta
589 and Delta virus using the plasma from the rhesus macaques immunized with circRNA^{RBD} vaccine.
590 In **e**, data were shown as the geometric mean ± geometric S.D., and each symbol represented an
591 individual mouse. The data were shown as the mean ± S.E.M. (n = 4). **f**, Measuring the SARS-
592 CoV-2 RBD-specific IFN-γ, IL-2 and IL-4 responses of PBMCs from rhesus macaques immunized
593 with circRNA^{RBD} vaccines via ELISPOT assay. In **f**, the data were shown as the mean ± S.E.M.
594 (n >= 2), and each symbol represented an individual rhesus macaque. **g**. Measuring the viral loads
595 (N gene) and subgenome RNA loads (E gene) in the lung tissues of challenged rhesus macaques.
596 In **g**, the data were shown as the mean ± S.E.M. (n = 4), and each symbol represented an individual
597 rhesus macaque. **h**, The HE staining of the pathological sections using the lung tissues from
598 immunized rhesus macaques at 7 days post SARS-CoV-2 virus challenges. **i**, The pathological
599 score of pneumonia based on the lung tissues from immunized rhesus macaques at 7 days post
600 SARS-CoV-2 challenges. The data were shown as the mean ± S.E.M. (n = 4), and each symbol
601 represented an individual rhesus macaque. **j**, Correlation of B cell response, T cell response and
602 pathological score in each immunized rhesus macaque. B cell responses were shown by the
603 neutralizing antibody production as value of NT50 against authentic SARS-CoV-2 virus. T cell
604 responses were shown as spots per 10^6 PBMCs detected in IFN-γ and IL-2 ELISpot assay.
605 Pathological scores were the same as in **i**.
606

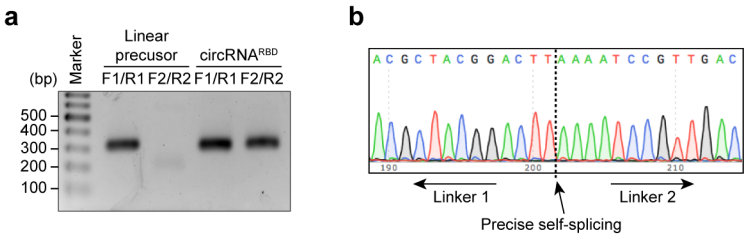

Extended Data Fig. 1 | PCR analysis to verify the precise circularization of circRNA. a, The agarose gel electrophoresis result of PCR analysis. Linear RNA precusor and circRNA^{RBD} were reverse transcription to cDNA, followed by PCR amplification with specific primers shown in **Fig 1a**. **b**, Sanger sequence result of the PCR products in (**a**).

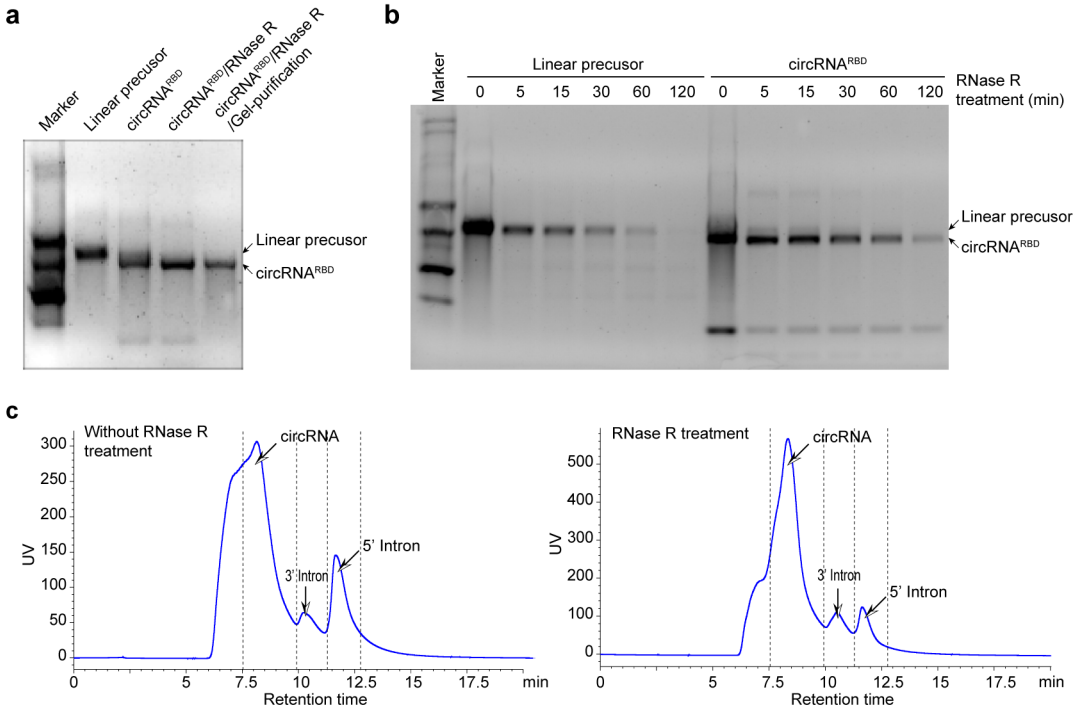

635

636 **Extended Data Fig. 2 | Agarose gel electrophoresis and HPLC purification of circRNA^{RBD}. a**,
637 The agarose gel electrophoresis result of linear RNA precusor and circRNA^{RBD} with different
638 treatments. **b**, The agarose gel electrophoresis result of circRNA^{RBD} and linear RNA precusor
639 digested by RNase R for various time from 5 min to 120 min. **c**, HPLC chromatogram of
640 circRNA^{RBD} without RNase R treatment (left) and circRNA^{RBD} treated by RNase R (right).

641

642

643

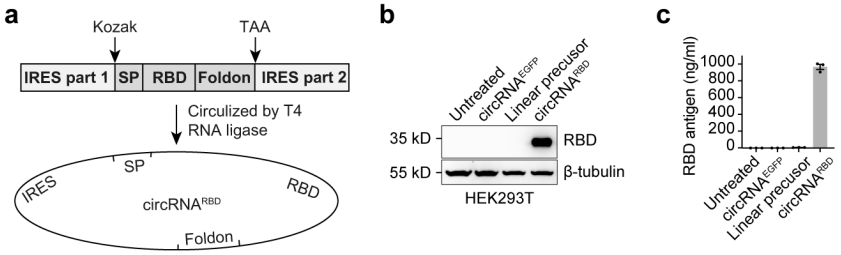

644

645

646 **Extended Data Fig. 3 | Expression of SARS-CoV-2 RBD antigens with circular RNAs**
647 **circulized by T4 RNA ligase. a**, Schematic diagram of circRNA^{RBD} circularization by the T4
648 RNA ligase. SP, signal peptide sequence of human tPA protein. Foldon, the trimerization domain
649 from bacteriophage T4 fibritin protein. RBD, the receptor binding domain of SARS-CoV-2 Spike
650 protein. **b**, Western Blot analysis showing the expression level of RBD antigens in the supernatant
651 of HEK293T cells transfected with circRNA^{RBD} circulized by the T4 RNA ligase. The
652 circRNA^{EGFP} and linear RNA precursor were used as controls. **c**, Measuring the concentration of
653 RBD antigens in the supernatant with quantitative ELISA assay. In **c**, data were shown as the mean
654 ± S.E.M. (n = 3).

655

656

657

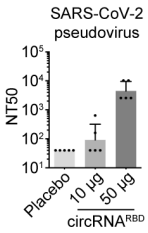

Extended Data Fig. 4 | Measuring the NT50 value of sera from mice immunized with cirRNA^{RBD} vaccine. The NT50 value was calculated using lentivirus-based SARS-CoV-2 pseudovirus. Data were shown as the geometric mean ± geometric S.D., and each symbol represented an individual mouse.

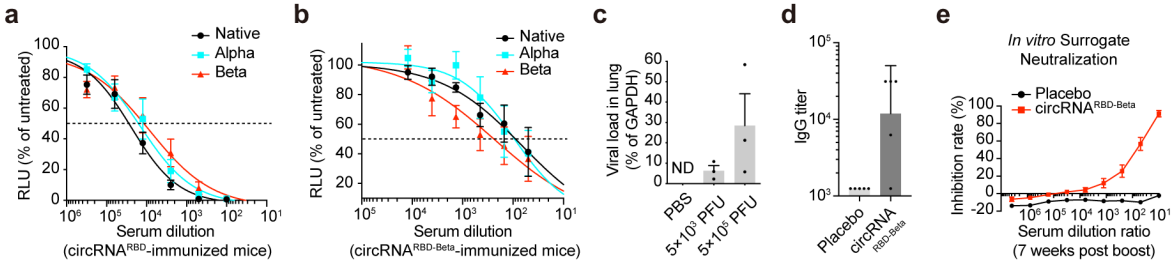

Extended Data Fig. 5 | SARS-CoV-2 circRNA$^{\text{RBD-Beta}}$ vaccine-elicited antibodies showed preferential neutralizing activity against Beta variant. a and **b**, Sigmoidal curve diagram of neutralization rate of VSV-based D614G, Alpha or Beta pseudovirus with the sera of mice immunized with circRNA^{RBD} or circRNA$^{\text{RBD-Beta}}$ vaccines. The data were shown as the mean ± S.E.M. (n = 4). Neutralization assay of the serum samples were collected at 1 week post boost. The data were shown as the mean ± S.E.M. (n = 5). **c**, Measuring the viral loads in the lung tissues of BALB/c mice infected by authentic SARS-CoV-2 Beta virus. The SARS-CoV-2 RNA copies were normalized with *GAPDH*. The data were shown as the mean ± S.E.M. (n = 3). **d**, Measuring the SARS-CoV-2 RBD-Beta-specific IgG endpoint GMTs with ELISA. In **d**, data were shown as the geometric mean ± geometric S.D., and each symbol represented an individual mouse. **e**, Sigmoidal curve diagram of the inhibition rate by sera from immunized mice with surrogate virus neutralization assay. In **e**, data were shown as the mean ± S.E.M. (n = 5). In **d** and **e**, the sera from circRNA$^{\text{RBD-Beta}}$ (50 μg) immunized mice were collected at 3 days before challenge with authentic SARS-CoV-2 Beta strain.

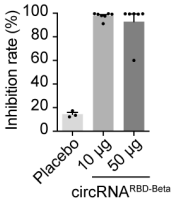

682

683 **Extended Data Fig. 6 | Measuring the neutralizing activity of sera from circRNA$^{RBD-Beta}$-**
684 **immunized mice with surrogate SARS-CoV-2 neutralization assay.** Instead of the lab-prepared
685 LNP, the commercial LNP (Precision Nanosystems) was used to encapsulate the circRNA$^{RBD-Beta}$
686 vaccine, and then the mice were immunized i.m. with 10 μg or 50 μg of new LNP-circRNA^{RBD-}
687 ^{Beta} vaccine at a two-week interval. The sera of immunized mice were collected at 2 weeks post the
688 second dose. The data were shown as the mean ± S.E.M. Each symbol represented an individual
689 mouse.

690

691

692

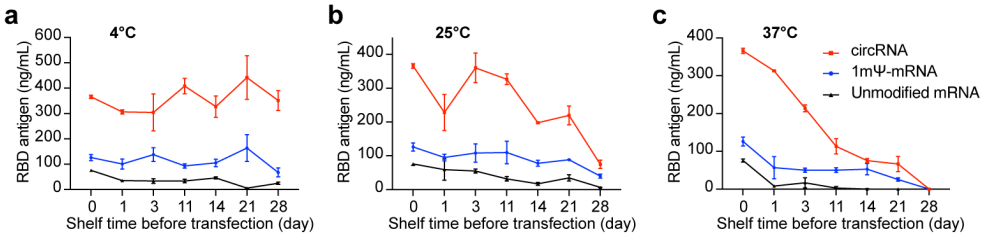

693 **Extended Data Fig. 7 | Measuring the expression level of RBD-Delta antigens in the**
694 **supernatant of HEK293T cells at different storage condition. a-c**, Using quantitative ELISA
695 to measure the expression level of RBD-Delta antigens in the supernatant of HEK293T cells
696 transfected with LNP-circRNA$^{\text{RBD-Delta}}$, LNP-1mΨ mRNA$^{\text{RBD-Delta}}$ and LNP-non-modified-
697 mRNA$^{\text{RBD-Delta}}$, stored at 4°C (**a**), 25°C (**b**) or 37°C (**c**). The LNP-RNA were stored at different
698 temperature and transfected at different time points. The data were shown as the mean ± S.E.M.
699 (n = 3).

700

701

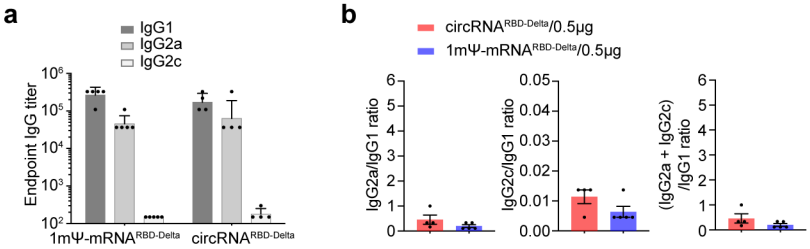

Extended Data Fig. 8 | The circRNA vaccine elicited stronger Th1-biased T cell immune responses than 1mΨ-mRNA vaccine. **a**, Measuring RBD-Delta-specific IgG1/IgG2a/IgG2c endpoint GMTs elicited by 0.5 μg of circRNA$^{RBD\text{-}Delta}$ vaccine or 1mΨ-mRNA$^{RBD\text{-}Delta}$ vaccine in mice. In **a**, data were shown as the geometric mean ± geometric S.D., and each symbol represented an individual mouse. **b**, Measuring the specific IgG2a/IgG1, IgG2c/IgG1 and (IgG2a + IgG2c)/IgG1 ratio of serum from mice immunized with 0.5 μg of circRNA$^{RBD\text{-}Delta}$ or 1mΨ mRNA$^{RBD\text{-}Delta}$. In **b**, data were shown as the mean ± S.E.M., and each symbol represented an individual mouse.

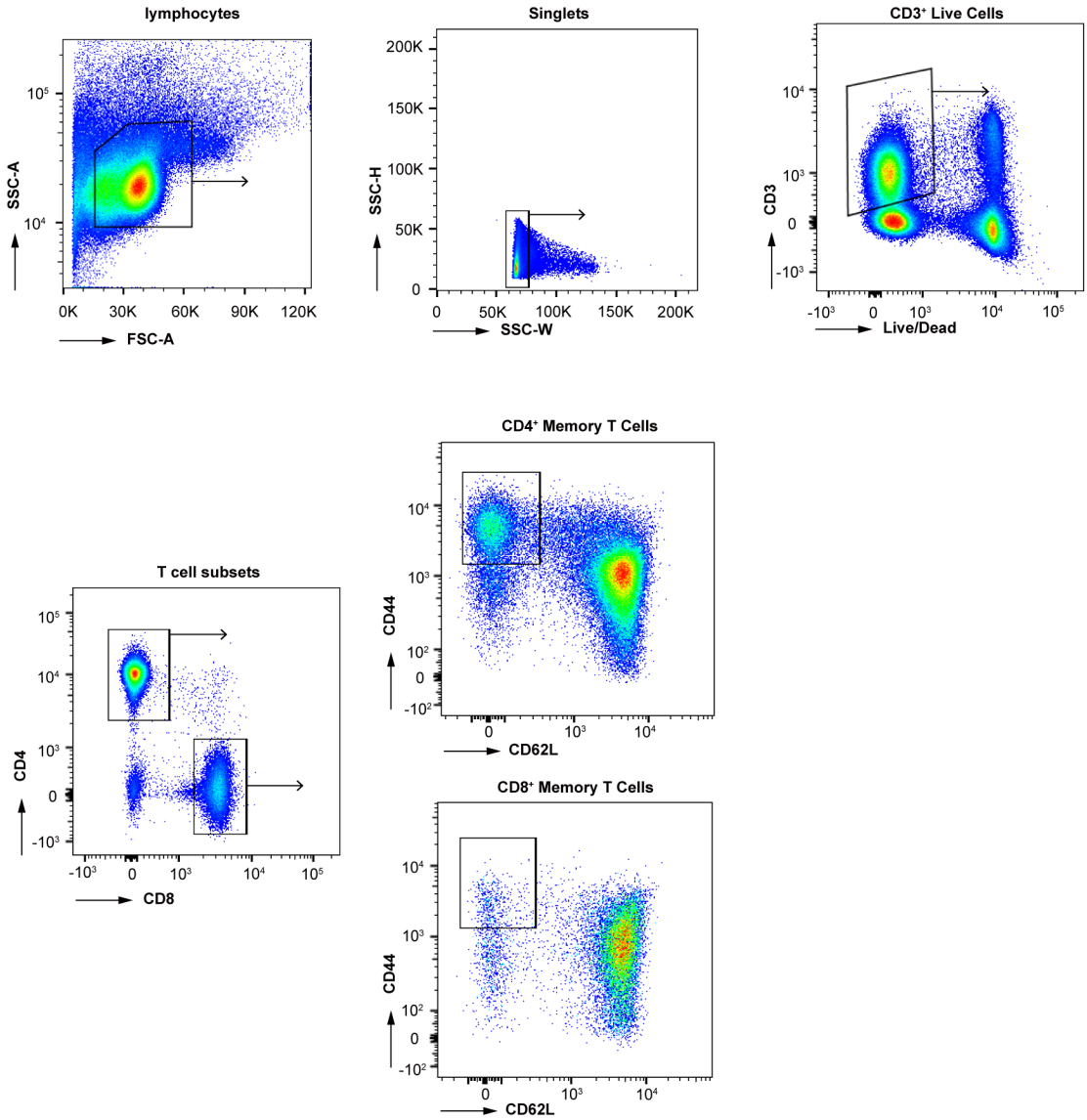

714

715 **Extended Data Fig. 9 | Flow panel and gating strategy to quantify SARS-CoV-2-RBD-specific**
716 **T cells in mice.** The plots showed the gating strategy of single and viable T cells in spleenocytes.
717 $CD4^+$ or $CD8^+$ Tem cells ($CD44^+CD62L^-$) were further analyzed for detecting the expression of
718 cytokines stimulated by corresponding RBD-Delta peptide pools.

719

720

721

722

723

724

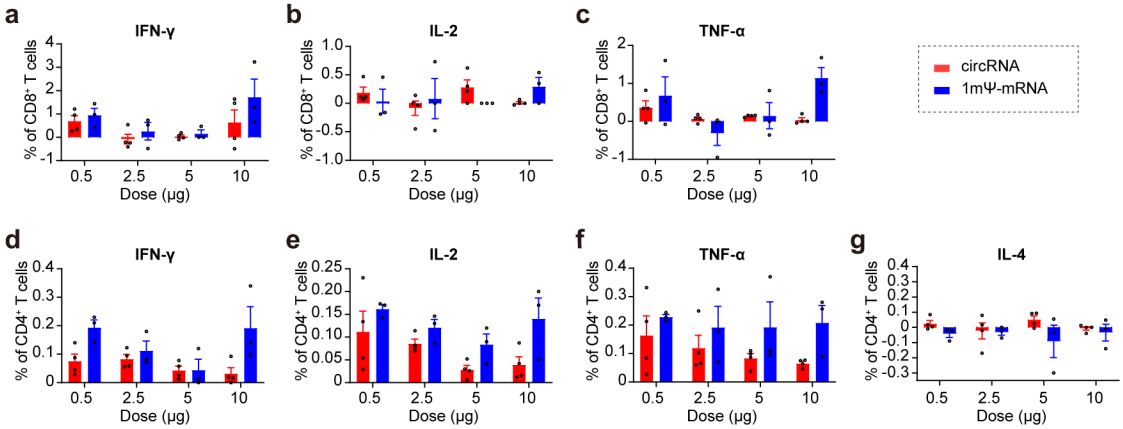

725

726 **Extended Data Fig. 10 | T cell immune responses elicited by SARS-CoV-2 circRNA$^{\text{RBD-Delta}}$**
727 **or mRNA$^{\text{RBD-Delta}}$ vaccines in mice. a-c**, The FACS analysis results showing the percentages of
728 CD8$^+$ Tem cells secreting IFN-γ (**a**), IL-2 (**b**), or TNF-α (**c**) after stimulated by RBD-Delta peptide
729 pools, respectively. **d-g**, The FACS analysis results showing the percentages of CD4$^+$ Tem cells
730 secreting IFN-γ (**d**), IL-2 (**e**), TNF-α (**f**) or IL-4 (**g**) after stimulated by RBD-Delta peptide pools,
731 respectively. In **a-g**, the data were presented as the mean ± S.E.M. (n = 3 or 4), and each symbol
732 represented an individual mouse.

733

734

735

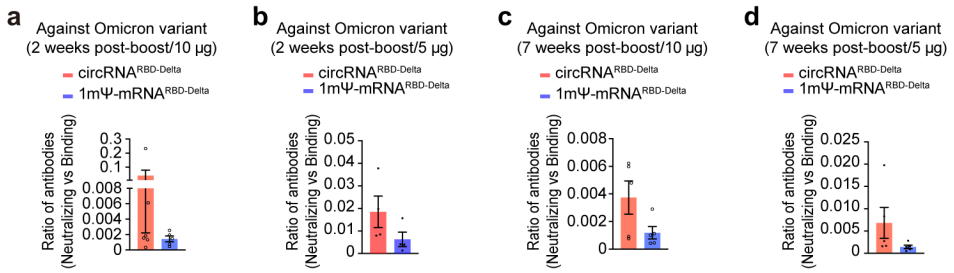

Extended Data Fig. 11 | The circRNA$^{\text{RBD-Delta}}$ vaccine elicited high-level of neutralizing antibodies against Omicron variant. **a** and **b**, Measuring the ratio of (Neutralizing antibodies)/(Binding antibodies) elicited by 10 μg (**a**) or 5 μg (**b**) of circRNA$^{\text{RBD-Delta}}$ vaccine or 1mΨ-mRNA$^{\text{RBD-Delta}}$ vaccine with the sera collected at 2 weeks post boost. The ratio of (NT50)/(Endpoint GMT) of each mouse was calculated. **c** and **d**, Measuring the ratio of (Neutralizing antibodies)/(Binding antibodies) elicited by 10 μg (**c**) or 5 μg (**d**) of circRNA$^{\text{RBD-Delta}}$ vaccine or 1mΨ-mRNA$^{\text{RBD-Delta}}$ vaccine with the sera collected at 7 weeks post boost. The ratio of (NT50)/(Endpoint GMT) of each mouse was calculated. In **a-d**, data were presented as the mean ± S.E.M., and each symbol represented an individual mouse.

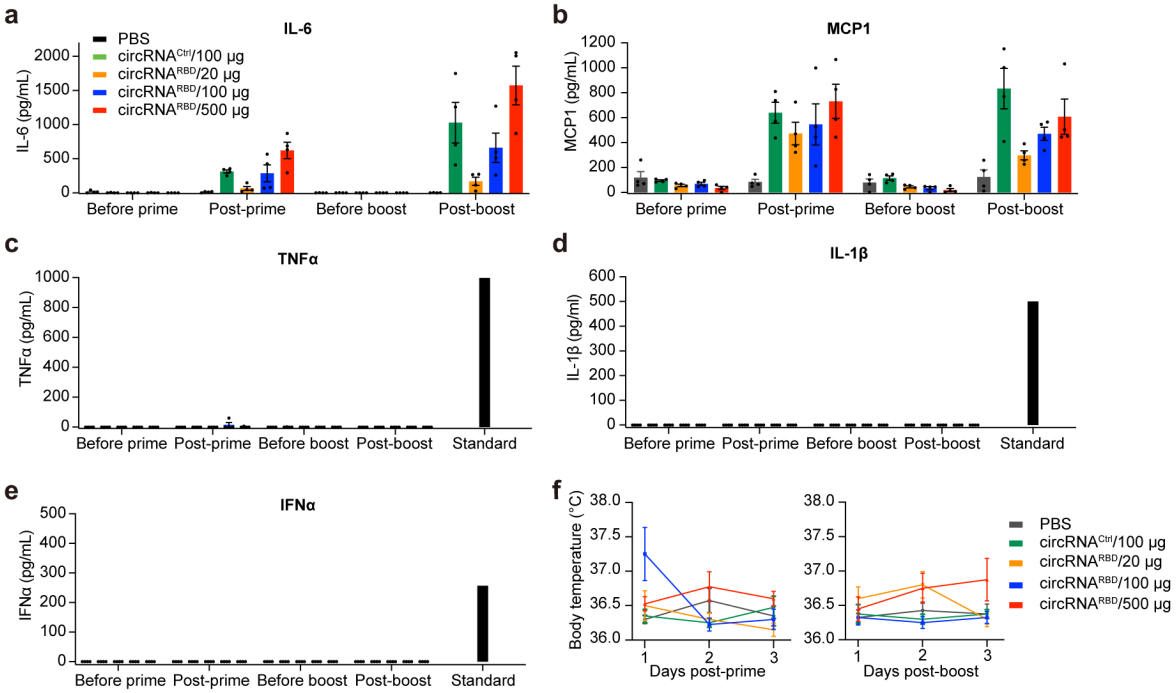

Extended Data Fig. 12 | CircRNA vaccine caused no obvious clinical signs of illness in rhesus macaques. a-e, Measuring the IL-6 (**a**), MCP1 (**b**), TNF-α (**c**), IL-1β (**d**) and IFN-α (**e**) level in the plasma of immunized rhesus macaques. **f**, Monitoring the body temperature of rhesus macaques. The body temperature is monitored within three days after the prime and boost dose. In **a-f**, data were shown as the mean ± S.E.M. (n = 4).

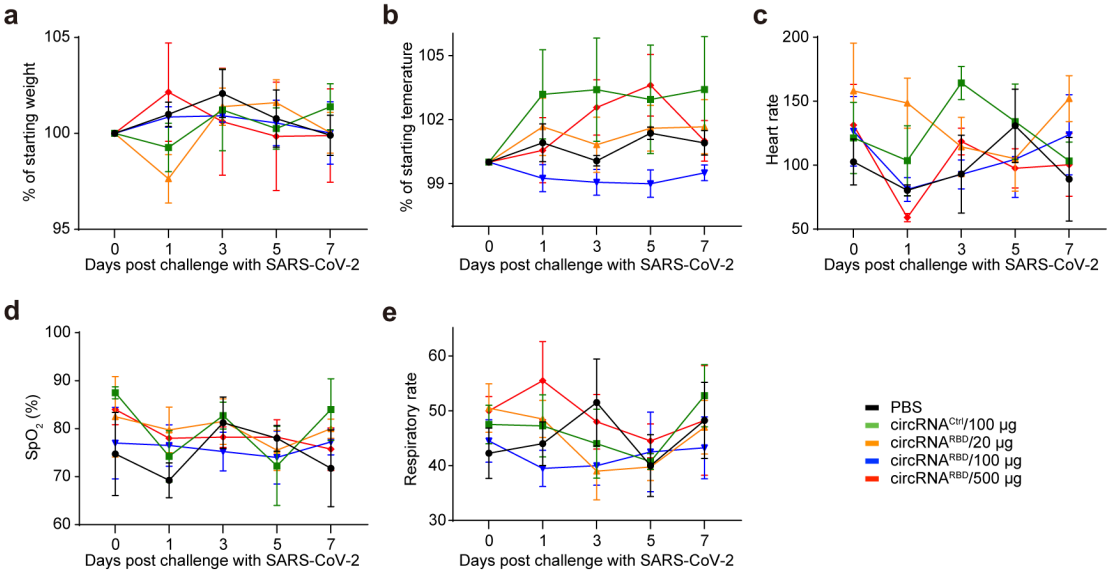

Extended Data Fig. 13 | Vital clinical signs of circRNA^{RBD}-immunized rhesus macaques after challenge with SARS-CoV-2. a-e, The body weight (**a**), temperature (**b**), heart rate (**c**), oxygen saturation (**d**), respiratory rate (**e**) were monitored after challenge with SARS-CoV-2 virus. In **a-e**, data were shown as the mean ± S.E.M. (n = 4).

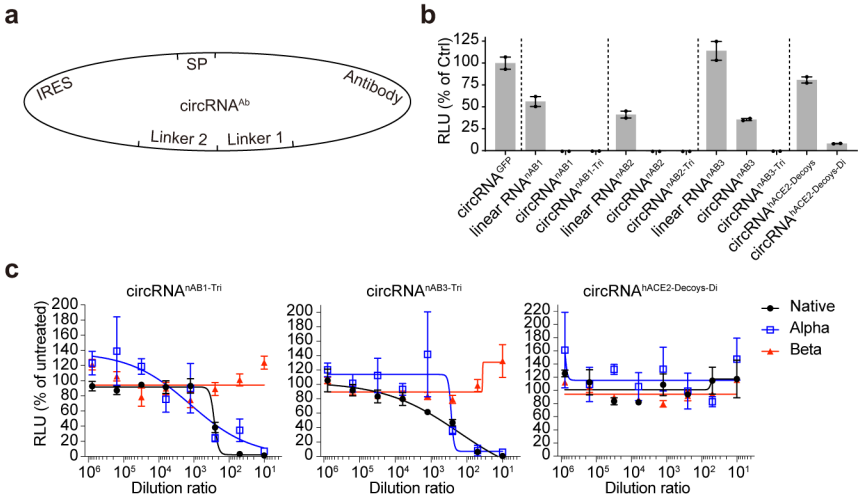

Extended Data Fig. 14 | Expression of SARS-CoV-2 neutralizing nanobodies or hACE2 decoys via circRNA platform. a, Schematic diagram of circRNA^{nAB} or circRNA$^{hACE2\ decoys}$ circularization by the Group I ribozyme autocatalysis. **b**, Lentivirial-based pseudovirus neutralization assay with the supernatant from cells transfected with circRNA encoding neutralizing nanobodies nAB1, nAB1-Tri, nAB2, nAB2-Tri, nAB3 and nAB3-Tri or ACE2 decoys. The nAB1-Tri, nAB2-Tri and nAB3-Tri represented the trimmer of nAB1, nAB2 and nAB3, respectively. The luciferase value was normalized to the circRNA^{EGFP} control. In **b**, data were shown as the mean ± S.E.M. (n = 2). **c**, Sigmoidal curve diagram of neutralization rate of VSV-based SARS-CoV-2 D614G, Alpha or Beta pseudovirus using the supernatant of cells transfected with neutralizing nanobodies nAB1-Tri, nAB3-Tri or ACE2 decoys encoded by the corresponding circRNAs. In **c**, data were shown as the mean ± S.E.M. (n = 3).

776 **Supplementary Table 1 | The peptide sequences of RBD-Delta antigen**

Serial No.	Sequence	Length (amino acid)
1	GIYQTSNFRVQPTESIVR	18
2	RVQPTESIVRFPNITNL	17
3	IVRFPNITNLCPFGEVF	17
4	TNLCPFGEVFNATRFASV	18
5	VFNATRFASVYAWNRKRI	18
6	SVYAWNRKRISNCVADY	17
7	KRISNCVADYSVLYNSA	17
8	ADYSVLYNSASFSTFKCY	18
9	SASFSTFKCYGVSPTKL	17
10	KCYGVSPTKLNDLCFTNV	18
11	KLNDLCFTNVYADSFVIR	18
12	NVYADSFVIRGDEVRQIA	18
13	IRGDEVRQIAPGQTGKIA	18
14	IAPGQTGKIADYNYKL	16
15	GKIADYNYKLPDDFTGCV	18
16	KLPDDFTGCVIAWNSNNL	18
17	CVIAWNSNNLDSKVGGNY	18
18	NLDSKVGGNYNYRYRLFR	18
19	NYNYRYRLFRKSNLKPF	17
20	LFRKSNLKPFERDISTEI	18
21	PFERDISTEIYQA	13
22	RDISTEIYQAGSKPCNGV	18
23	YQAGSKPCNGVEGFNCYF	18
24	NGVEGFNCYFPLQSYGF	17
25	CYFPLQSYGFQPTNGVGY	18
26	GFQPTNGVGYQPYRVVVL	18
27	GYQPYRVVVLSFELLHA	17
28	VVLSFELLHAPATVCGPK	18
29	HAPATVCGPKKSTNLVK	17
30	GPKKSTNLVKNKCVNFNF	18
31	VKNKCVNFNFNGLTGTGV	18

777

778 **Supplementary Table 2 | The peptide sequences of RBD antigen**

Serial No.	Sequence	Length (amino acid)
1	GIYQTSNFRVQPTESIVR	18
2	RVQPTESIVRFPNITNL	17
3	IVRFPNITNLCPFGEVF	17
4	TNLCPFGEVFNATRFASV	18
5	VFNATRFASVYAWNRKRI	18
6	SVYAWNRKRISNCVADY	17
7	KRISNCVADYSVLYNSA	17
8	ADYSVLYNSASFSTFKCY	18
9	SASFSTFKCYGVSPTKL	17
10	KCYGVSPTKLNDLCFTNV	18
11	KLNDLCFTNVYADSFVIR	18
12	NVYADSFVIRGDEVRQIA	18
13	IRGDEVRQIAPGQTGKIA	18
14	IAPGQTGKIADYNYKL	16
15	GKIADYNYKLPDDFTGCV	18
16	KLPDDFTGCVIAWNSNNL	18
17	CVIAWNSNNLDSKVGGNY	18
18	NLDSKVGGNYNYLYRLFR	18
19	NYNYLYRLFRKSNLKPF	17
20	LFRKSNLKPFERDISTEI	18
21	PFERDISTEIYQA	13
22	RDISTEIYQAGSTPCNGV	18
23	YQAGSTPCNGVEGFNCYF	18
24	NGVEGFNCYFPLQSYGF	17
25	CYFPLQSYGFQPTNGVGY	18
26	GFQPTNGVGYQPYRVVVL	18
27	GYQPYRVVVLSFELLHA	17
28	VVLSFELLHAPATVCGPK	18
29	HAPATVCGPKKSTNLVK	17
30	GPKKSTNLVKNKCVNFNF	18
31	VKNKCVNFNFNGLTGTGV	18

779
780
781
782
783

784 **References**

785 1 Wu, F. *et al.* A new coronavirus associated with human respiratory disease in China. *Nature* **579**, 265-269,
786 doi:10.1038/s41586-020-2008-3 (2020).
787 2 Zhou, P. *et al.* A pneumonia outbreak associated with a new coronavirus of probable bat origin. *Nature*
788 **579**, 270-273, doi:10.1038/s41586-020-2012-7 (2020).
789 3 Dejnirattisai, W. *et al.* SARS-CoV-2 Omicron-B.1.1.529 leads to widespread escape from neutralizing
790 antibody responses. *Cell*, doi:10.1016/j.cell.2021.12.046 (2022).
791 4 Cao, Y. *et al.* Omicron escapes the majority of existing SARS-CoV-2 neutralizing antibodies. *Nature*,
792 doi:10.1038/d41586-021-03796-6 (2021).
793 5 Liu, L. *et al.* Striking antibody evasion manifested by the Omicron variant of SARS-CoV-2. *Nature*,
794 doi:10.1038/d41586-021-03826-3 (2021).
795 6 Planas, D. *et al.* Considerable escape of SARS-CoV-2 Omicron to antibody neutralization. *Nature*,
796 doi:10.1038/d41586-021-03827-2 (2021).
797 7 Cele, S. *et al.* Omicron extensively but incompletely escapes Pfizer BNT162b2 neutralization. *Nature*,
798 doi:10.1038/d41586-021-03824-5 (2021).
799 8 Cameroni, E. *et al.* Broadly neutralizing antibodies overcome SARS-CoV-2 Omicron antigenic shift.
800 *Nature*, doi:10.1038/d41586-021-03825-4 (2021).
801 9 V'Kovski, P., Kratzel, A., Steiner, S., Stalder, H. & Thiel, V. Coronavirus biology and replication:
802 implications for SARS-CoV-2. *Nat Rev Microbiol* **19**, 155-170, doi:10.1038/s41579-020-00468-6 (2021).
803 10 Kim, D. *et al.* The Architecture of SARS-CoV-2 Transcriptome. *Cell* **181**, 914-921 e910,
804 doi:10.1016/j.cell.2020.04.011 (2020).
805 11 Hoffmann, M. *et al.* SARS-CoV-2 Cell Entry Depends on ACE2 and TMPRSS2 and Is Blocked by a
806 Clinically Proven Protease Inhibitor. *Cell* **181**, 271-280 e278, doi:10.1016/j.cell.2020.02.052 (2020).
807 12 Yan, R. *et al.* Structural basis for the recognition of SARS-CoV-2 by full-length human ACE2. *Science*
808 **367**, 1444-1448, doi:10.1126/science.abb2762 (2020).
809 13 Wrapp, D. *et al.* Cryo-EM structure of the 2019-nCoV spike in the prefusion conformation. *Science* **367**,
810 1260-1263, doi:10.1126/science.abb2507 (2020).
811 14 Shang, J. *et al.* Cell entry mechanisms of SARS-CoV-2. *Proc Natl Acad Sci U S A* **117**, 11727-11734,
812 doi:10.1073/pnas.2003138117 (2020).
813 15 Walls, A. C. *et al.* Structure, Function, and Antigenicity of the SARS-CoV-2 Spike Glycoprotein. *Cell* **181**,
814 281-292 e286, doi:10.1016/j.cell.2020.02.058 (2020).
815 16 Hsieh, C. L. *et al.* Structure-based design of prefusion-stabilized SARS-CoV-2 spikes. *Science* **369**, 1501-
816 1505, doi:10.1126/science.abd0826 (2020).
817 17 Bangaru, S. *et al.* Structural analysis of full-length SARS-CoV-2 spike protein from an advanced vaccine
818 candidate. *Science* **370**, 1089-1094, doi:10.1126/science.abe1502 (2020).
819 18 Krammer, F. SARS-CoV-2 vaccines in development. *Nature* **586**, 516-527, doi:10.1038/s41586-020-2798-
820 3 (2020).

821 19 Mullard, A. COVID-19 vaccine development pipeline gears up. *Lancet* **395**, 1751-1752,
822 doi:10.1016/S0140-6736(20)31252-6 (2020).
823 20 Gao, Q. *et al.* Development of an inactivated vaccine candidate for SARS-CoV-2. *Science* **369**, 77-81,
824 doi:10.1126/science.abc1932 (2020).
825 21 van Doremalen, N. *et al.* ChAdOx1 nCoV-19 vaccine prevents SARS-CoV-2 pneumonia in rhesus
826 macaques. *Nature* **586**, 578-582, doi:10.1038/s41586-020-2608-y (2020).
827 22 Sanchez-Felipe, L. *et al.* A single-dose live-attenuated YF17D-vectored SARS-CoV-2 vaccine candidate.
828 *Nature* **590**, 320-325, doi:10.1038/s41586-020-3035-9 (2021).
829 23 Zhu, F. C. *et al.* Safety, tolerability, and immunogenicity of a recombinant adenovirus type-5 vectored
830 COVID-19 vaccine: a dose-escalation, open-label, non-randomised, first-in-human trial. *Lancet* **395**, 1845-1854,
831 doi:10.1016/S0140-6736(20)31208-3 (2020).
832 24 Yang, J. *et al.* A vaccine targeting the RBD of the S protein of SARS-CoV-2 induces protective immunity.
833 *Nature* **586**, 572-577, doi:10.1038/s41586-020-2599-8 (2020).
834 25 Dai, L. *et al.* A Universal Design of Betacoronavirus Vaccines against COVID-19, MERS, and SARS. *Cell*
835 **182**, 722-733 e711, doi:10.1016/j.cell.2020.06.035 (2020).
836 26 Yu, J. *et al.* DNA vaccine protection against SARS-CoV-2 in rhesus macaques. *Science* **369**, 806-811,
837 doi:10.1126/science.abc6284 (2020).
838 27 Corbett, K. S. *et al.* SARS-CoV-2 mRNA vaccine design enabled by prototype pathogen preparedness.
839 *Nature* **586**, 567-571, doi:10.1038/s41586-020-2622-0 (2020).
840 28 Corbett, K. S. *et al.* Evaluation of the mRNA-1273 Vaccine against SARS-CoV-2 in Nonhuman Primates.
841 *N Engl J Med* **383**, 1544-1555, doi:10.1056/NEJMoa2024671 (2020).
842 29 Zhang, N. N. *et al.* A Thermostable mRNA Vaccine against COVID-19. *Cell* **182**, 1271-1283 e1216,
843 doi:10.1016/j.cell.2020.07.024 (2020).
844 30 Laczko, D. *et al.* A Single Immunization with Nucleoside-Modified mRNA Vaccines Elicits Strong
845 Cellular and Humoral Immune Responses against SARS-CoV-2 in Mice. *Immunity* **53**, 724-732 e727,
846 doi:10.1016/j.immuni.2020.07.019 (2020).
847 31 Huang, Q. *et al.* A single-dose mRNA vaccine provides a long-term protection for hACE2 transgenic mice
848 from SARS-CoV-2. *Nat Commun* **12**, 776, doi:10.1038/s41467-021-21037-2 (2021).
849 32 Sahin, U. *et al.* COVID-19 vaccine BNT162b1 elicits human antibody and TH1 T cell responses. *Nature*
850 **586**, 594-599, doi:10.1038/s41586-020-2814-7 (2020).
851 33 Vogel, A. B. *et al.* BNT162b vaccines protect rhesus macaques from SARS-CoV-2. *Nature*,
852 doi:10.1038/s41586-021-03275-y (2021).
853 34 Pardi, N., Hogan, M. J., Porter, F. W. & Weissman, D. mRNA vaccines - a new era in vaccinology. *Nat*
854 *Rev Drug Discov* **17**, 261-279, doi:10.1038/nrd.2017.243 (2018).
855 35 Jackson, N. A. C., Kester, K. E., Casimiro, D., Gurunathan, S. & DeRosa, F. The promise of mRNA
856 vaccines: a biotech and industrial perspective. *NPJ Vaccines* **5**, 11, doi:10.1038/s41541-020-0159-8 (2020).

857 36 Durymanov, M. & Reineke, J. Non-viral Delivery of Nucleic Acids: Insight Into Mechanisms of
858 Overcoming Intracellular Barriers. *Front Pharmacol* **9**, 971, doi:10.3389/fphar.2018.00971 (2018).
859 37 Fenton, O. S. *et al.* Bioinspired Alkenyl Amino Alcohol Ionizable Lipid Materials for Highly Potent In
860 Vivo mRNA Delivery. *Adv Mater* **28**, 2939-2943, doi:10.1002/adma.201505822 (2016).
861 38 Wesselhoeft, R. A. *et al.* RNA Circularization Diminishes Immunogenicity and Can Extend Translation
862 Duration In Vivo. *Mol Cell* **74**, 508-520 e504, doi:10.1016/j.molcel.2019.02.015 (2019).
863 39 Chen, Y. G. *et al.* N6-Methyladenosine Modification Controls Circular RNA Immunity. *Mol Cell* **76**, 96-
864 109 e109, doi:10.1016/j.molcel.2019.07.016 (2019).
865 40 Zhang, X. O. *et al.* Complementary sequence-mediated exon circularization. *Cell* **159**, 134-147,
866 doi:10.1016/j.cell.2014.09.001 (2014).
867 41 Chen, L. L. The biogenesis and emerging roles of circular RNAs. *Nat Rev Mol Cell Biol* **17**, 205-211,
868 doi:10.1038/nrm.2015.32 (2016).
869 42 Kristensen, L. S. *et al.* The biogenesis, biology and characterization of circular RNAs. *Nat Rev Genet* **20**,
870 675-691, doi:10.1038/s41576-019-0158-7 (2019).
871 43 Memczak, S. *et al.* Circular RNAs are a large class of animal RNAs with regulatory potency. *Nature* **495**,
872 333-338, doi:10.1038/nature11928 (2013).
873 44 Enuka, Y. *et al.* Circular RNAs are long-lived and display only minimal early alterations in response to a
874 growth factor. *Nucleic Acids Res* **44**, 1370-1383, doi:10.1093/nar/gkv1367 (2016).
875 45 Legnini, I. *et al.* Circ-ZNF609 Is a Circular RNA that Can Be Translated and Functions in Myogenesis.
876 *Mol Cell* **66**, 22-37 e29, doi:10.1016/j.molcel.2017.02.017 (2017).
877 46 Zhang, M. *et al.* A novel protein encoded by the circular form of the SHPRH gene suppresses glioma
878 tumorigenesis. *Oncogene* **37**, 1805-1814, doi:10.1038/s41388-017-0019-9 (2018).
879 47 Zhang, M. *et al.* A peptide encoded by circular form of LINC-PINT suppresses oncogenic transcriptional
880 elongation in glioblastoma. *Nat Commun* **9**, 4475, doi:10.1038/s41467-018-06862-2 (2018).
881 48 Gao, X. *et al.* Circular RNA-encoded oncogenic E-cadherin variant promotes glioblastoma tumorigenicity
882 through activation of EGFR-STAT3 signalling. *Nat Cell Biol*, doi:10.1038/s41556-021-00639-4 (2021).
883 49 Wesselhoeft, R. A., Kowalski, P. S. & Anderson, D. G. Engineering circular RNA for potent and stable
884 translation in eukaryotic cells. *Nat Commun* **9**, 2629, doi:10.1038/s41467-018-05096-6 (2018).
885 50 Yang, Y. *et al.* Extensive translation of circular RNAs driven by N(6)-methyladenosine. *Cell Res* **27**, 626-
886 641, doi:10.1038/cr.2017.31 (2017).
887 51 Kou, Y. *et al.* Tissue plasminogen activator (tPA) signal sequence enhances immunogenicity of MVA-
888 based vaccine against tuberculosis. *Immunol Lett* **190**, 51-57, doi:10.1016/j.imlet.2017.07.007 (2017).
889 52 Richner, J. M. *et al.* Modified mRNA Vaccines Protect against Zika Virus Infection. *Cell* **169**, 176,
890 doi:10.1016/j.cell.2017.03.016 (2017).
891 53 Pardi, N. *et al.* Zika virus protection by a single low-dose nucleoside-modified mRNA vaccination. *Nature*
892 **543**, 248-251, doi:10.1038/nature21428 (2017).

893 54 Bouwman, K. M. *et al.* Multimerization- and glycosylation-dependent receptor binding of SARS-CoV-2
894 spike proteins. *PLoS Pathog* **17**, e1009282, doi:10.1371/journal.ppat.1009282 (2021).
895 55 Papanikolopoulou, K., van Raaij, M. J. & Mitraki, A. Creation of hybrid nanorods from sequences of
896 natural trimeric fibrous proteins using the fibritin trimerization motif. *Methods Mol Biol* **474**, 15-33,
897 doi:10.1007/978-1-59745-480-3_2 (2008).
898 56 Ou, X. *et al.* Characterization of spike glycoprotein of SARS-CoV-2 on virus entry and its immune cross-
899 reactivity with SARS-CoV. *Nat Commun* **11**, 1620, doi:10.1038/s41467-020-15562-9 (2020).
900 57 Montagutelli, X. *et al.*, doi:10.1101/2021.03.18.436013 (2021).
901 58 Chen, Q. *et al.* Transient acquisition of cross-species infectivity during the evolution of SARS-CoV-2. *Natl*
902 *Sci Rev* **8**, nwab167, doi:10.1093/nsr/nwab167 (2021).
903 59 Gu, H. *et al.* Adaptation of SARS-CoV-2 in BALB/c mice for testing vaccine efficacy. *Science* **369**, 1603-
904 1607, doi:10.1126/science.abc4730 (2020).
905 60 Lustig, Y. *et al.* Neutralising capacity against Delta (B.1.617.2) and other variants of concern following
906 Comirnaty (BNT162b2, BioNTech/Pfizer) vaccination in health care workers, Israel. *Euro Surveill* **26**,
907 doi:10.2807/1560-7917.ES.2021.26.26.2100557 (2021).
908 61 Torgovnick, J. Effectiveness of Covid-19 Vaccines against the B.1.617.2 (Delta) Variant. *N Engl J Med*
909 **385**, e92, doi:10.1056/NEJMc2113090 (2021).
910 62 Planas, D. *et al.* Reduced sensitivity of SARS-CoV-2 variant Delta to antibody neutralization. *Nature* **596**,
911 276-280, doi:10.1038/s41586-021-03777-9 (2021).
912 63 Fischer, J. W. & Leung, A. K. CircRNAs: a regulator of cellular stress. *Crit Rev Biochem Mol Biol* **52**, 220-
913 233, doi:10.1080/10409238.2016.1276882 (2017).
914 64 Graham, B. S. Rapid COVID-19 vaccine development. *Science* **368**, 945-946, doi:10.1126/science.abb8923
915 (2020).
916 65 Dowd, K. A. & Pierson, T. C. Antibody-mediated neutralization of flaviviruses: a reductionist view.
917 *Virology* **411**, 306-315, doi:10.1016/j.virol.2010.12.020 (2011).
918 66 Halstead, S. B. & O'Rourke, E. J. Dengue viruses and mononuclear phagocytes. I. Infection enhancement
919 by non-neutralizing antibody. *J Exp Med* **146**, 201-217, doi:10.1084/jem.146.1.201 (1977).
920 67 Rey, F. A., Stiasny, K., Vaney, M. C., Dellarole, M. & Heinz, F. X. The bright and the dark side of human
921 antibody responses to flaviviruses: lessons for vaccine design. *EMBO Rep* **19**, 206-224,
922 doi:10.15252/embr.201745302 (2018).
923 68 Takano, T., Yamada, S., Doki, T. & Hohdatsu, T. Pathogenesis of oral type I feline infectious peritonitis
924 virus (FIPV) infection: Antibody-dependent enhancement infection of cats with type I FIPV via the oral route. *J Vet*
925 *Med Sci* **81**, 911-915, doi:10.1292/jvms.18-0702 (2019).
926 69 Wen, J. *et al.* Antibody-dependent enhancement of coronavirus. *Int J Infect Dis* **100**, 483-489,
927 doi:10.1016/j.ijid.2020.09.015 (2020).
928 70 Dejnirattisai, W. *et al.* Cross-reacting antibodies enhance dengue virus infection in humans. *Science* **328**,
929 745-748, doi:10.1126/science.1185181 (2010).

930 71 Martinez-Vega, R. A., Carrasquila, G., Luna, E. & Ramos-Castaneda, J. ADE and dengue vaccination.
931 *Vaccine* **35**, 3910-3912, doi:10.1016/j.vaccine.2017.06.004 (2017).
932 72 Sette, A. & Crotty, S. Adaptive immunity to SARS-CoV-2 and COVID-19. *Cell* **184**, 861-880,
933 doi:10.1016/j.cell.2021.01.007 (2021).
934 73 Xiang, Y. *et al.* Versatile and multivalent nanobodies efficiently neutralize SARS-CoV-2. *Science* **370**,
935 1479-1484, doi:10.1126/science.abe4747 (2020).
936 74 Schoof, M. *et al.* An ultrapotent synthetic nanobody neutralizes SARS-CoV-2 by stabilizing inactive Spike.
937 *Science* **370**, 1473-1479, doi:10.1126/science.abe3255 (2020).
938 75 Linsky, T. W. *et al.* De novo design of potent and resilient hACE2 decoys to neutralize SARS-CoV-2.
939 *Science* **370**, 1208-1214, doi:10.1126/science.abe0075 (2020).
940 76 Muik, A. *et al.* Neutralization of SARS-CoV-2 lineage B.1.1.7 pseudovirus by BNT162b2 vaccine-elicited
941 human sera. *Science*, doi:10.1126/science.abg6105 (2021).
942 77 Wang, Z. *et al.* mRNA vaccine-elicited antibodies to SARS-CoV-2 and circulating variants. *Nature*,
943 doi:10.1038/s41586-021-03324-6 (2021).
944 78 Wang, P. *et al.* Antibody Resistance of SARS-CoV-2 Variants B.1.351 and B.1.1.7. *Nature*,
945 doi:10.1038/s41586-021-03398-2 (2021).
946 79 Karim, S. S. A. & Karim, Q. A. Omicron SARS-CoV-2 variant: a new chapter in the COVID-19 pandemic.
947 *Lancet* **398**, 2126-2128, doi:10.1016/S0140-6736(21)02758-6 (2021).
948 80 Cao, Y. *et al.* Potent Neutralizing Antibodies against SARS-CoV-2 Identified by High-Throughput Single-
949 Cell Sequencing of Convalescent Patients' B Cells. *Cell* **182**, 73-84 e16, doi:10.1016/j.cell.2020.05.025 (2020).
950 81 Du, S. *et al.* Structurally Resolved SARS-CoV-2 Antibody Shows High Efficacy in Severely Infected
951 Hamsters and Provides a Potent Cocktail Pairing Strategy. *Cell* **183**, 1013-1023 e1013,
952 doi:10.1016/j.cell.2020.09.035 (2020).
953 82 Barnes, C. O. *et al.* SARS-CoV-2 neutralizing antibody structures inform therapeutic strategies. *Nature*
954 **588**, 682-687, doi:10.1038/s41586-020-2852-1 (2020).
955 83 Koenig, P. A. *et al.* Structure-guided multivalent nanobodies block SARS-CoV-2 infection and suppress
956 mutational escape. *Science* **371**, doi:10.1126/science.abe6230 (2021).
957 84 Tai, W. *et al.* A novel receptor-binding domain (RBD)-based mRNA vaccine against SARS-CoV-2. *Cell*
958 *Res* **30**, 932-935, doi:10.1038/s41422-020-0387-5 (2020).
959 85 Routhu, N. K. *et al.* SARS-CoV-2 RBD trimer protein adjuvanted with Alum-3M-052 protects from
960 SARS-CoV-2 infection and immune pathology in the lung. *Nat Commun* **12**, 3587, doi:10.1038/s41467-021-23942-
961 y (2021).
962 86 Khan, K. *et al.* Omicron infection enhances neutralizing immunity against the Delta variant. *medRxiv*,
963 doi:10.1101/2021.12.27.21268439 (2021).
964 87 Liu, C. X. *et al.* RNA circles with minimized immunogenicity as potent PKR inhibitors. *Mol Cell*,
965 doi:10.1016/j.molcel.2021.11.019 (2021).

966 88 Chan, K. K. *et al.* Engineering human ACE2 to optimize binding to the spike protein of SARS coronavirus
967 2. *Science* **369**, 1261-1265, doi:10.1126/science.abc0870 (2020).
968 89 Glasgow, A. *et al.* Engineered ACE2 receptor traps potently neutralize SARS-CoV-2. *Proc Natl Acad Sci*
969 *U S A* **117**, 28046-28055, doi:10.1073/pnas.2016093117 (2020).
970 90 Boutros, C. *et al.* Safety profiles of anti-CTLA-4 and anti-PD-1 antibodies alone and in combination. *Nat*
971 *Rev Clin Oncol* **13**, 473-486, doi:10.1038/nrclinonc.2016.58 (2016).
972 91 He, X. & Xu, C. Immune checkpoint signaling and cancer immunotherapy. *Cell Res* **30**, 660-669,
973 doi:10.1038/s41422-020-0343-4 (2020).
974 92 Sabapathy, K. & Lane, D. P. Therapeutic targeting of p53: all mutants are equal, but some mutants are
975 more equal than others. *Nat Rev Clin Oncol* **15**, 13-30, doi:10.1038/nrclinonc.2017.151 (2018).
976 93 Mukhopadhyay, S., Vander Heiden, M. G. & McCormick, F. The Metabolic Landscape of RAS-Driven
977 Cancers from biology to therapy. *Nat Cancer* **2**, 271-283, doi:10.1038/s43018-021-00184-x (2021).
978

979

Acknowledgements

We acknowledge C. Dong and X. Wang (Tsinghua University) for providing fluorescent-conjugated antibodies. We thank J. Xiao (Peking University) for providing purified SARS-CoV-2 Spike proteins. We thank J. Yan (Institute of Microbiology, Chinese Academy of Sciences) for providing RBD peptide pools. We thank the Laboratory Animal Centre of Peking University for the feeding of mice. We thank the HPLC Core at the National Center for Protein Sciences at Peking University (Beijing), particularly H. Li and G. Li for technical help. We thank the flow cytometry Core at the National Center for Protein Sciences at Peking University (Beijing), particularly H. Lv, Y. Guo, H. Yang, F. Wang for technical help. This project was supported by funds from National Key R&D Program of China (2020YFA0707800 to W.W., 2020YFA0707600 to Z.Z.); Beijing Municipal Science & Technology Commission (Z181100001318009); the National Science Foundation of China (31930016); Beijing Advanced Innovation Center for Genomics at Peking University and the Peking-Tsinghua Center for Life Sciences (to W.W.); the National Science Foundation of China (31870893); the National Major Science & Technology Project for Control and Prevention of Major Infectious Diseases in China (2018ZX10301401 to Z.Z.) and the Fellowship of China National Postdoctoral Program for Innovative Talents (BX20200010, to L.Q.).

Author contributions

W.W. conceived and supervised this project. W.W., L.Q., Z.Y. and Y.S. designed the experiments. L.Q., Z.Y., Y.S., L.L., F.C., Y.X., Z.W., H.T., A.Y., and X.X. performed the experiments with the help from X.Z., F.T., C.W., X.D., L.G., S.L., C.Y., C.T., Y.Y., W.Y., J.W., Y.Z., Q.H., Z.Z., Y.C., Y.W., X.P., J.W., and X.S.X.. L.Q., Z.Y., Y.S. and W.W. wrote the manuscript with the help of all other authors.

Competing interests

Patents have been filed relating to the data presented in this manuscript.

1008 **Methods**

1009 **Plasmids construction.** The SARS-CoV-2 RBD antigen, EGFP, nanobody or hACE2-decoy-
1010 coding sequence was PCR amplified and cloned into the pcircRNA-EV backbone and constructed
1011 the corresponding pcircRNA plasmids for the following IVT (*in vitro* transcription).

1012

1013 **Cell culture.** HEK293T, NIH3T3 and Huh-7 cell lines were maintained in our laboratory. The
1014 HEK293T-hACE2 cell line was ordered from Biodragon Inc. (#BDAA0039, Beijing, China). The
1015 A549-hACE2 cell line was generated in our laboratory. These mammalian cell lines were cultured
1016 in Dulbecco′ s Modified Eagle Medium (Corning, 10-013-CV) with 10% fetal bovine serum
1017 (FBS) (BI), supplemented with 1% penicillin-streptomycin in 5% CO_2 incubator at 37°C. The
1018 Huh-7 cells were cultured with the methods previously described[80].

1019

1020 **circRNA transfection *in vitro*.** For the circRNA transfection in HEK293T or NIH3T3 cells, 3×10^5
1021 cells per well were seeded in 12-well plates. 2 μg of circRNAs were transfected into the HEK293T
1022 or NIH3T3 cells, using Lipofectamine MessengerMax (Invitrogen, LMRNA003) according to the
1023 manufacturer's instructions. At 24-48 hr post transfection, the cell lysis and supernatant were
1024 collected for the following detections.

1025

1026 **Quantitative determination of SARS-CoV-2 Spike RBD expression in vitro.** Quantification of
1027 RBD expression in cell culture supernatants was performed with a commercial SARS-CoV-2
1028 Spike RBD Protein ELISA kit (ABclonal, #RK04135) according to the manufacturer's instruction.
1029 The supernatants were diluted at 1:500 rate. Final concentrations of RBD were calculated basing
1030 on the linear standard curve of absorbance at 450 nm, using 630 nm as reference. Briefly, the
1031 detection wells were pre-coated with monoclonal antibody specific for Spike RBD protein. After
1032 incubation with samples or standards at 37°C for two hours, samples unbound to immobilized
1033 antibody would be removed by washing steps. Then the RBD-specific antibodies were added to
1034 wells for one-hour incubation at 37°C. After washing, the HRP substrates and stop solution were
1035 added and the absorbance at 450 nm were measured using 630 nm as reference.

1036

1037 **Mouse vaccination and serum collection.** The BALB/c mice were ordered from Beijing Vital
1038 River Laboratory Animal Technology Co., Ltd. All mice were bred and kept under SPF (specific
1039 pathogen-free) conditions in the Laboratory Animal Center of Peking University. The animal
1040 experiments were approved by Peking University Laboratory Animal Center (Beijing), and
1041 undertaken in accordance with the National Institute of Health Guide for Care and Use of
1042 Laboratory Animals. All the animal experiments with SARS-CoV-2 challenge were conducted
1043 under animal biosafety level 3 (ABSL3) facilities in Institute of Pathogen Biology, Chinese
1044 Academy of Medical Sciences. All the animal experiments with SARS-CoV-2 challenge were
1045 reviewed and approved by the Committee on the Ethics of Animal Experiments of Institute of
1046 Pathogen Biology, Chinese Academy of Medical Sciences.
1047 For mouse vaccination, groups of 6-8 week-old female BLAB/c mice were intramuscularly
1048 immunized with LNP-circRNA^{RBD} or Placebo (Empty LNP) in 100 μL using a 1 mL sterile syringe,
1049 and 2 or 3 weeks later a second dose was immunized to boost the immune responses. The sera of
1050 immunized mice were collected to detect the SARS-CoV-2-specific IgG endpoint GMTs and
1051 neutralizing antibodies as described below.
1052
1053 **Antibody endpoint GMT measurement with ELISA.** All the immunized mouse serum samples
1054 were heat-inactivated at 56°C for 30 min before use. The SARS-CoV-2-specific IgG antibody
1055 endpoint GMT was measured by ELISA. Briefly, serial 3-fold dilutions (in 1% BSA) of heat-
1056 inactivated sera, starting at 1:100, were added to the 96-well plates (100 μL/well; Costar) coated
1057 with recombinant SARS-CoV-2 Spike or RBD antigens (Sino Biological) and blocked with 1%
1058 BSA for 60 min at 37°C. Then, after three washes with wash buffer, the Horseradish peroxidase
1059 HRP-conjugated rabbit anti-mouse IgG (Sigma) diluted in 1% BSA at 1:10,000 ratio, was added
1060 to the plates and incubated at 37°C for 30 min. Then the plates were washed for 3 times with wash
1061 buffer and added with TMB substrates (100 μL/well) followed by incubation for 15-20 min. And
1062 then the ELISA stop buffer was added into the plates. Finally, the absorbance (450/630 nm) was
1063 measured with Infinite M200 (TECAN). The IgG endpoint GMTs were defined as the dilution
1064 fold, which emitted an optical density exceeding 3x background (without serum but the secondary
1065 antibody was added).
1066

1067 **SARS-CoV-2 Surrogate Virus Neutralization Assay.** The neutralizing activity of mouse serum
1068 samples was detected by SARS-CoV-2 Surrogate Virus Neutralization Test Kit (L00847A,
1069 GenScript). Detections were performed according to manufacturer's instruction. Serial 10-fold
1070 dilutions of heat-inactivated sera, starting at 1:10, were incubated with HRP-conjugated RBD
1071 solutions at 37°C for half an hour, and then the mixtures were added into 96-well plates pre-coated
1072 with human ACE2 (hACE2) proteins and incubated for 15 min at 37°C. After washing the TMB
1073 substrates and stop solutions were added and the absorbance (450/630 nm) was measured with
1074 Infinite M200 (TECAN). The inhibition rates of serum samples were calculated according to the
1075 following formula. The 50% neutralization geometric mean titer (NT50) was determined using
1076 four-parameter nonlinear regression in Prism 8 (GraphPad).
1077 Inhibition rate = (1- OD value of sample/OD value of negative control) × 100%
1078
1079 **Pseudovirus-based neutralization assay.** The production of lentivirus-based SARS-CoV-2
1080 pseudovirus and neutralization assay were performed as described previously[94]. Briefly, the
1081 SARS-CoV-2 pseudovirus were produced by co-transfecting plasmids psPAX2 (6 μg), pSpike (6
1082 μg), and pLenti-Luc-GFP (6 μg) into HEK293T cells using X tremeGENE HP DNA Transfection
1083 Reagent (Roche) according to the manufacturer′s instructions. 48 hr post transfection, the
1084 supernatants containing pseudovirus particles were harvested and filtered through a 0.22-μm
1085 sterilized membrane for the neutralization assay as described below.
1086 For the determination of NT50 of immunized mouse serum, the HEK293T-hACE2 cells were
1087 seeded in 96-well plates (50,000 cells/well) and incubated for approximate 24 hr until reaching
1088 over 90% confluent, preparing for pseudovirus infection. The mouse serum was 3-fold diluted,
1089 starting at 1:40, and incubated with the SARS-CoV-2 pseudovirus (MOI ≈ 0.05) at 37°C for 60
1090 min. The DMEM medium without serum was used as the negative control group. Then the
1091 supernatant of HEK293T-hACE2 cells were removed and the mixer of serum and pseudovirus
1092 were added to each well. 36-48 hr later, the luciferase activity, which reflecting the degree of
1093 SARS-CoV-2 pseudovirus transfection, was measured using the Nano-Glo Luciferase Assay
1094 System (Promega). The NT50 was defined as the fold-dilution, which emitted an exceeding 50%
1095 inhibition of pseudovirus infection in comparison with the control group.
1096 The neutralization assay of VSV-based pseudovirus of SARS-CoV-2 and variants was
1097 performed as described previously[80,81]. Briefly, the sera were serially diluted using complete

1098 DMEM culture media in 96-well white plates for a total of six gradients, and then the virus solution
1099 with ~1.3×10^4 TCID50 was added. The complete DMEM medium was used as the control group.
1100 After one hour incubation in 5% CO_2 incubator at 37°C, the 96-well white plates were added with
1101 Huh7 cells (100 μL/well), which were adjusted to a concentration of 2×10^5 cells/mL. After 24 h
1102 incubation in 5% CO_2 incubator at 37°C, the culture supernatant was aspirated gently to leave 100
1103 μL in each well, and then 100 μL of luciferase substrate (Perkinelmer, 6066769) was added to each
1104 well for the detection of luminescence using Infinite M200 (TECAN). Relative luciferase units
1105 (RLU) were normalized to corresponding DMEM control group, and the NT50 were determined
1106 by a four-parameter nonlinear regression in Prism (GraphPad).
1107 For the neutralization assay of circRNA^{nAB} or circRNA$^{ACE2\ decoys}$, the HEK293T-hACE2 cells
1108 were seeded in 96-well plates (50,000 cells/well) and incubated for approximate 24 hr until
1109 reaching over 90% confluent. The pseudovirus were pre-incubated with the supernatant of the
1110 circRNA^{nAB} or circRNA$^{ACE2\ decoys}$ transfected cells at 37°C for 60 min, and then added to cells in
1111 the 96-well plates. Media were changed at 24 hr after transduction. All cells were collected at 48
1112 hr after transduction. Luciferase activity was measured using the Nano-Glo Luciferase Assay
1113 System (Promega). The relative luminescence units were normalized to cells infected with
1114 supernatant of cell transfected with the circRNA^{EGFP}.
1115
1116 **Authentic SARS-CoV-2 NT50 Assay.** A549-hACE2 cells were seeded in 96-well plates (20,000
1117 cells/well) and incubated for approximately 24 hr until 90-100% confluent. The mouse serum was
1118 5-fold serially diluted in DMEM, starting at 1:10. The diluted sera were then mixed with titrated
1119 virus in a 1:1 (vol/vol) ratio to generate a mixture containing ~2,000 PFU/well of viruses (MOI =
1120 0.1), followed by an incubation at 37°C for 1 hr. Then the virus/sera mixtures were added to 24-
1121 well plates of A549-ACE2 cells, supplemented with 100 μL of DMEM containing 10% FBS in
1122 each well. The supernatant and cell pellet precipitation were then collected, and the viral load was
1123 detected by RT-qPCR. Briefly, the RNA was extracted from the cell pellet and reverse transcribed.
1124 SARS-CoV-2 RNA quantification was performed by RT-qPCR targeting the N gene of SARS-
1125 CoV-2 using Roche LightCycler® 96. The abundance of *GAPDH* was set as internal reference.
1126 The NT50 was defined as the fold-dilution, which emitted an exceeding 50% inhibition of infection
1127 in comparison with the control group.
1128

1129 **Mouse challenge experiments.** The mouse model for SARS-CoV-2 Beta variant challenge has
1130 previously been characterized[57]. The BALB/c mice immunized with circRNA$^{RBD\text{-}Beta}$ (50 μg) were
1131 challenged with 5×10^4 PFU SARS-CoV-2 Beta variant at 7 weeks post boost. The body weight of
1132 mice were recorded daily. At 3 days post challenge, the immunized mice were sacrificed, and their
1133 lung tissues were collected to measure the viral RNA load, as described below.
1134
1135 **Quantification of viral load in the lung tissues of challenged BALB/c mice by RT-qPCR.** The
1136 viral RNA load in the lung tissues of challenged mice was detected by quantitative RT-qPCR.
1137 Briefly, the lung tissues were collected and homogenized with stainless steel beads in TRIZOL (1
1138 ml for each sample). The RNAs in tissues were then extracted and reverse transcribed. SARS-
1139 CoV-2 RNA quantification was performed by RT-qPCR targeting the N gene of SARS-CoV-2,
1140 using Roche LightCycler® 96. The abundance of *GAPDH* was set as internal reference. The
1141 placebo group viral load was normalized to 100%.
1142
1143 **T cell flow cytometry analysis.** The Splenocytes from each immunized mouse were cultured in
1144 R10 media (RPMI 1640 supplemented with 1% Pen-Strep antibiotic, 10% HI-FBS), stimulated
1145 with RBD peptide pools (**Supplementary Table 1**) at a final concentration of 2 μg/mL for each
1146 peptide. 3 hr later, the Golgi Stop transport inhibitor cocktail (BD) was added according to
1147 manufacturer instructions. And then, 6 hr later, cells from each group were pooled for stimulation
1148 with cell stimulation cocktail (PMA/Ionomycin) as a positive control. Following stimulation, cells
1149 were washed with PBS prior to staining with LIVE/DEAD for 20 min at room temperature. Cells
1150 were then washed in stain buffer (PBS supplemented with 2.5% FBS) and suspended in Fc Block
1151 for 5 min at RT prior to staining with a surface stain of following antibodies: CD3 (Invitrogen, 45-
1152 0031-82)/CD4 (BD, 562285)/CD8 (BD, 553035) /CD44 (BD, 563058)/CD62L (BD, 560507).
1153 After 20 min, cells were washed with stain buffer, and then fixed and permeabilized using the BD
1154 Cytoperm fixation/permeabilization solution kit according to manufacturer instructions. Cells
1155 were washed in perm/wash solution, followed by intracellular staining (30 min, RT) using a
1156 cocktail of the following antibodies: IFN-γ (BD, 557998)/IL-2 (BD, 560547)/IL-4 (BD,
1157 554435)/TNF-α (BD, 557644). Finally, cells were washed in perm/wash solution and suspended
1158 in stain buffer. Samples were washed and acquired on a LSRFortessa (BD Biosciences). Analysis
1159 was performed using FlowJo software.

1160

1161 **Ethics and biosafety statement.** All rhesus macaques experiments were performed in the animal
1162 biosafety level 4 (ABSL-4) facility of National Kunming High-level Biosafety Primate Research
1163 Center, Yunnan, China. All animal procedures were approved by the Institutional Animal Care
1164 and Use Committee of Institute of Medical Biology, Chinese Academy of Medical Science. Rhesus
1165 macaques were monitored at least twice daily throughout the experiment. Commercial monkey
1166 chow, treats and fruit were provided daily by trained personnel.

1167

1168 **Rhesus macaque vaccination and plasma collection.** For the vaccination of rhesus macaque,
1169 groups of 2~4-year-old rhesus macaques were immunized with LNP-circRNA^{RBD} (20 μg, N= 4;
1170 100 μg, N= 4; 500 μg, N= 4), LNP-circRNA^{Ctrl} (circRNA without the RBD-encoding sequence;
1171 100 μg, N= 4) or PBS (N= 4) in 300 μL (>300 μL in 500 μg dose group) via intramuscular injection
1172 in the quadriceps muscle (prime: left, boost: right) twice at a three-week interval. The plasma of
1173 immunized rhesus macaques were collected at 0, 1 and 14 days post the prime, and 0, 1, 14, 28
1174 and 35 days post the boost.

1175

1176 **SARS-CoV-2 Virus amplification and identification.** Viral stock of native SARS-CoV-2 was
1177 obtained from the Center of Diseases Control, Guangdong Province China. Viruses were amplified
1178 on Vero-E6 cells and concentrated by ultrafilter system via 300 kD module (Millipore). Amplified
1179 SARS-CoV-2 were confirmed via RT-PCR, sequencing and transmission electronic microscopy,
1180 and titrated via plaque assay (10^6 pfu/ml).

1181

1182 **ELISpot assay.** The T cell immune responses in rhesus macaques were detected using the PBMCs
1183 with commercially available NHP IFN-γ and IL-2 ELISpot assay kits (Mabtech), and NHP IL-4
1184 ELISpot assay kit (U-CyTech). The cryopreserved rhesus macaques PBMCs were thawed and
1185 cultured with pre-warmed AIM-V media. For IFN-γ, IL-2 and IL-4 ELISpot assay, 1.0×10^5
1186 PBMCs were stimulated with final concentration of 1 μg/mL for each RBD peptide
1187 (**Supplementary Table 2**). The test for each rhesus macaque were performed in two or three
1188 technical repetitions. The dimethyl sulphoxide (DMSO) served as un-stimulated control, and the
1189 Phytohemagglutinin (PHA-P, Sigma) and CELL STIMULATION COCKTAIL (ThermoFisher)
1190 were used as positive controls. After 24h of stimulation with RBD peptide pools, the streptavidin-

1191 HRP substrate (for IFN-γ and IL-2) or AEC substrate (IL-4) were added into plate. The spots were
1192 counted by Beijing Dakewei Biotechnology Co., Ltd. The results are background (DMSO treated
1193 group) subtracted and normalized to SFC/10^6 PBMCs.
1194
1195 **SARS-CoV-2 challenge in rhesus macaques.** At 5 weeks post boost, all the immunized rhesus
1196 macaques were challenged with 1.0×10^6 PFU of native SARS-CoV-2 virus via the intranasal (0.5
1197 ml) and intratracheal (0.5 ml) routes. The plasma of rhesus macaques was collected and vital
1198 clinical signs were recorded on 0, 1, 3, 5 and 7 days post virus challenge. At 7 days post virus
1199 challenge, all rhesus macaques were sacrificed to collect specimen for further experiments.
1200
1201 **Histopathology.** On the 7 days post virus challenge, the rhesus monkeys were euthanized, and
1202 necropsies were performed according to standard protocols. After the dissection, a general
1203 examination of the main organs was performed. The lung tissues were harvested, fixed in 10%
1204 neutral formalin buffer and embedded in paraffin. 2 μm tissue sections were prepared. Slides were
1205 stained with Hematoxylin and Eosin (H&E). The slide images were collected by using Pannoramic
1206 DESK and analyzed with Caseviewer C.V 2.3 and Image-Pro Plus 6.0. Histopathological analysis
1207 of tissue slides was scored by 3 independent pathologists blinded to the groups of animals.
1208
1209 **Cytokines analyses.** The plasma of rhesus monkeys were isolated 24 hr post prime or boost and
1210 diluted in 5-fold or 10-fold. All plasma samples were detected using following ELISA kits: IL-6
1211 (Abcam, ab242233), MCP-1 (Cloud-cline corp, SEA087Si96T), TNF-α (Abcam, ab252354), IL-
1212 1β (Cloud-cline Corp, SEA563Si96T) and IFN-α (Chenglin, AD0081Mk) according to the
1213 manufacturer's instructions.

1214 **Statistics.** An unpaired two-sided Student's t-test was performed for comparison as indicated in
1215 the figure legends. Statistical analyses were performed with Prism 8 (GraphPad Software, Inc.).

1216 **Reporting Summary.** Further information on research design is available in the Nature Research
1217 Reporting Summary linked to this article.

Data availability

All data and materials presented in this manuscript are available from the corresponding author (W.W.) upon a reasonable request under a completed Material Transfer Agreement.

References

94 Pinto, D. *et al.* Cross-neutralization of SARS-CoV-2 by a human monoclonal SARS-CoV antibody. *Nature* **583**, 290-295, doi:10.1038/s41586-020-2349-y (2020).